Panx1 deletion promotes synaptic reconfiguration and recruitment of cell death pathways in the Zebrafish MPTP model

***Authors**:* Georg S.O. Zoidl[1,3], Nickie Safarian[1,4], Christiane Zoidl[1,2], Steven Connor[1,3], Georg R. Zoidl[1,2,3]

Affiliations: [1] Department of Biology, [2] Department of Psychology, [3] Center for Integrated and Applied Neuroscience (CIAN), York University, [4] Department of Genomics and Genome Biology, Sick Kids Hospital, Toronto, Canada.

Corresponding Author: Georg R. Zoidl, gzoidl@yorku.ca

27 ***Graphical Abstract***

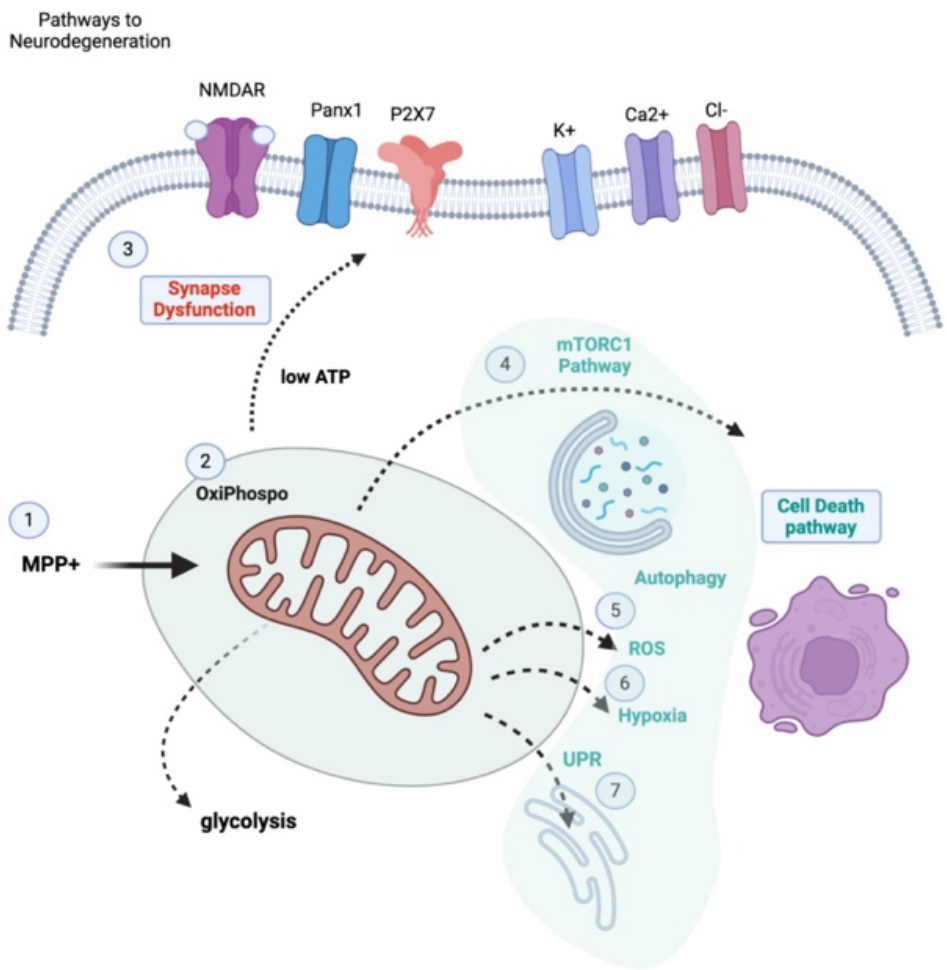

28

29

30 ***Highlights***

31 • A genetic model was combined with the MPTP neurotoxin to explore the roles of
32 zebrafish Pannexin-1 channels in neurodegeneration.
33
34 • A dysregulation of Alzheimer's, Parkinson's, Amyotrophic Lateral Sclerosis (ALS), and
35 Huntington's disease biomarkers, suggested a protective role of Panx1a ablation.
36
37 • The potential beneficial impact of targeting Panx1a is superseded by synaptic plasticity
38 loss, dysfunctional mitochondrial metabolism, and cell death.
39

40 ***Abstract***

41 Pannexin-1 (Panx1) channels have garnered attention for their implications in neurodegeneration,
42 potentially with a role in mediating the delicate balance between cell death and survival.
43 However, a comprehensive understanding of the underlying molecular and cellular mechanisms
44 remains elusive, and whether Panx1 exhibits dual protective and toxic roles throughout the
45 lifespan remains to be determined. To address these gaps, we focused on early-life changes in
46 zebrafish larvae with impaired Panx1a function subjected to acute 1-methyl-4-phenyl-1,2,3,6-
47 tetrahydropyridine (MPTP) treatment. We demonstrate that a single four-hour exposure to MPTP
48 induces substantial alterations in locomotor behavior, the transcriptome, and local field potentials
49 within the ascending visual pathway. KEGG pathway analysis underscored MPTP's regulatory
50 influence on neurodegeneration; here the differential expression of biomarkers for Alzheimer's,
51 Parkinson's, Amyotrophic Lateral Sclerosis (ALS), and Huntington's disease, suggested a
52 protective role of Panx1a ablation. However, the potential beneficial impact of targeting Panx1a
53 is superseded by the deregulation of oxidative phosphorylation, glycolysis, ROS, hypoxia,
54 unfolded protein response pathways, and reduced extracellular ATP. Notably, these changes
55 correlate with a loss of synaptic neurotransmitter receptor and ion channel/transaporter
56 expression and the differential expression of mTORC1, autophagy, and apoptosis signaling
57 pathways. The resultant cell death was demonstrated by acridine orange dye uptake and in-vivo
58 imaging, with a pronounced loss of cells observed in the pallium and tectum regions. Dual
59 recordings of local field potentials across the optic tectum and pallium demonstrate Panx1a's
60 involvement in modulating local neuronal networks. Collectively, our results shed light on the
61 impacts of acute MPTP treatment on locomotor behavior, transcriptomic shifts, metabolic
62 disturbances, and the pivotal role of Panx1a in neurodegeneration and cell death. These insights
63 enhance our comprehension of the intricate molecular and cellular mechanisms underpinning

64 neurodegeneration, with implications for potential therapeutic strategies targeting Panx1 channels
65 in the context of neuroinflammatory pathologies.
66
67
68 ***Introduction***

69 Neurodegenerative diseases (NDDs) like Alzheimer's Disease (AD), Parkinson's Disease,
70 (PD), or Amyotrophic Lateral Sclerosis (ALS) significantly burden individuals worldwide, with
71 their diverse manifestations impacting millions of lives. As the prevalence of NDDs continues to
72 rise and healthcare costs soar, addressing the challenges they present has become a critical
73 priority. Though diverse in presentation, different forms of NDDs often share common hallmarks
74 upon the onset of clinical symptoms. They include the aggregation of pathological proteins,
75 synaptic and neuronal network dysfunction, proteostasis disturbances, cytoskeletal abnormalities,
76 disrupted energy homeostasis, DNA and RNA defects, inflammation, and neuronal cell death.
77 These changes culminate in the progressive loss of neurons, leading to impaired memory,
78 cognition, behavior, sensory functions, and motor abilities [1]. At the most fundamental level we
79 must ask whether NDDs emerge from common insults derailing the homeostasis of the nervous
80 system at an asymptomatic stage, and how time, duration, and context of the initial changes
81 dictate outcomes.

82 Mitochondrial energy metabolism and calcium dysregulation occur early in many NDDs,
83 including Alzheimer's disease, Parkinson's disease, Huntington's disease, and other outcomes [2,3].
84 These dysfunctions appear to be genetically preprogrammed, striking initially the weakest, and
85 most sensitive points of the nervous system. In addition to ATP production, mitochondria are an
86 epicenter of many metabolic pathways and important cellular functions, including the fine-tuning
87 of intracellular calcium ($_iCa^{2+}$) signaling, regulation of cell death, lipid synthesis, ROS signaling,

88 and cellular quality control [4]. Disruption in mitochondrial function and metabolism appears to
89 underlie several NDDs such as AD, PD, HD, and others [5]. This suggests that mitochondrial
90 metabolic defects may be drivers or even initiators of the neurodegenerative process [6].
91 Mechanistically, at least some of the common NDD pathways outlined above converge on
92 Pannexin-1 (Panx1) which may play a central role in early life changes influencing the onset and
93 development of NDDs. Panx1 is a member of the pannexin gene family encompassing three
94 glycosylated integral membrane proteins (Panx1-Panx3) [7-10]. The Panx1 protein can form large-
95 pore ATP-release channels, enabling paracrine and intercellular communication within the
96 nervous system [11]. Additionally, a small-pore variant of heptameric Panx1 channels exists,
97 although its functional roles have yet to be determined [12,13].
98 Recent studies have highlighted Panx1's roles during neurodevelopment and its potential
99 involvement in NDDs [14-16]. Panx1 channels are expressed in neurons and glial cells, including
100 microglia cells and astrocytes, as well as in the neurovascular unit [17-20]. Panx1 channels play
101 critical roles in cell death [21-25], calcium signaling [26,27], neurotoxicity regulation [28,29], non-synaptic
102 communication [30,31], inflammation [22,32,33], neuronal excitability [34] and endema[35]. The relevance of
103 Panx1's interaction with the cytoskeleton and whether this interaction contributes to cytoskeletal
104 abnormalities in NDDs remains to be explored [36,37]. Dysregulated Panx1 activity can exacerbate
105 pathological processes, and increased neuronal excitability has been associated with neurological
106 disorders such as Alzheimer's Disease, ALS, and epilepsy [38-40]. In mouse models, the loss of
107 Panx1 function caused learning and memory deficits, impaired social interactions, and
108 diminished bioelectrical properties of the brain [41,42]. Notably, our interest in studying Panx1
109 functions early in life coincides with the expression peak at birth after a rise during perinatal
110 stages [19].

111 To investigate early in-live roles of Panx1 when mitochondrial function and metabolism
112 are disrupted, we treated six-day-old Tubingen Longfin (TL) larvae with 1-methyl-4-phenyl-
113 1,2,3,6-tetrahydropyridine (MPTP) to induce rapid neurotoxicity [43]. We leveraged multiple
114 advantages of zebrafish models as a translational model for fundamental process discovery.
115 Zebrafish have a remarkable degree of ≈ 70% genetic similarity with humans that extends to
116 genes associated with NDDs. The zebrafish Panx1a gene is 72% identical to human Panx1. The
117 simple vertebrate nervous system develops rapidly in a transparent body, which facilitates direct
118 assessment of the impact of MPTP on critical stages of neurodevelopment *ex utero.* Testable
119 visual-motor behaviors develop early in life in larvae and MPTP treatment is non-invasive and
120 applied through tank water.

121 We demonstrate that an acute treatment with MPTP induced rapid neurotoxicity; RNA-
122 seq analysis showed that a four-hour treatment applied to TL larvae (Panx1a$^{+/+}$) initiated
123 transcriptome-wide expression changes indicating metabolic dysfunction, impaired proteostasis,
124 neurodegeneration, reduced extracellular ATP, and cell death. MPTP treatment also caused a
125 dose-dependent reduction of swimming behavior.

126 Next, the in-house generated Panx1 knockout zebrafish line Panx1a$^{-/-}$ was used to test the
127 hypothesis that the zebrafish Panx1a ohnologue of mammalian Panx1 acts as a regulatory sensor,
128 akin to a rheostat, for programmed cell death. Our previous research using this Panx1a$^{-/-}$ line has
129 demonstrated that global depletion of Panx1a channels in 6dpf zebrafish larvae caused
130 visuomotor deficiencies associated with dopaminergic signaling alterations [44]. By contrasting
131 how MPTP affected the Panx1a$^{-/-}$ and parental Panx1a$^{+/+}$ strains, RNA-seq and a computational
132 Gene Set Expression Analysis (GSEA) [45] demonstrated that in low ATP conditions Panx1a
133 ablation caused a modulation of NDD hallmark genes, such as the reduced differential expression
134 of the functional homologs of mammalian alpha-Synuclein or the microtubule-associated Tau

135 proteins. The reduced expression of the NDD hallmark genes coincided with enhanced
136 differential expression of pathways regulating oxidative phosphorylation, cell death, lipid
137 synthesis, ROS signaling, and cellular quality control, influencing cell survival. Further, ablation
138 of Panx1 altered the molecular composition of synapses; the expression of pre- and post-synaptic
139 genes including but not limited to major neurotransmitter receptors, and anion and cation
140 channels were downregulated, suggesting a major impairment of synaptic function. The study of
141 *in-vivo* recorded local field potentials (LFPs) from the optic tectum and the dorsomedial (DM)
142 region of the pallium further demonstrated that the synapse alterations caused neuronal network
143 dysfunctions. The testing of swimming behavior showed that the genetic ablation of Panx1
144 worsened impairments during a metabolic crisis.

145 Collectively, our study offers first-time insights into the molecular and cellular events
146 underlying early-stage NDDs, explicitly focusing on Panx1's role in PD-like neurodegeneration.
147 By leveraging the advantages of gene-edited zebrafish larvae as a model organism and by using
148 acute treatment with MPTP, we have made significant strides in understanding the functional
149 consequences of Panx1 manipulation, providing evidence that the loss of Panx1 causes a
150 reduction of key hallmarks of NDDs. However, we must recognize that targeting Panx1 during an
151 experimentally induced metabolic crisis has severe consequences, such as synaptic and neuronal
152 network dysfunction, aberrant proteostasis, altered energy homeostasis, and neuronal cell death.
153 Our results will contribute to a better understanding of the roles of Panx1 as a regulatory sensor
154 in the complex mechanisms causing NDDs.

155

156 **Results**

157 ***Acute treatment with MPTP altered the locomotion of zebrafish larvae.***

158 Pharmacological targeting of mitochondrial metabolism in dopaminergic neurons through
159 acute MPTP treatment was evaluated to establish a practical alternative – a single acute treatment
160 for 4 hours during a critical developmental stage – to substitute chronic MPTP treatments, and to
161 investigate initial stages leading to NDDs. The six-days post fertilization (6dpf) timepoint was
162 chosen based on the expression profile of Panx1 genes in rodents and fish; the expression reaches
163 a transient peak before birth in rodents [19], and when zebrafish transition to free-swimming
164 juveniles.

165 To assess the impact of MPTP treatment, we utilized a modified visual-motor response
166 (VMR) assay, measuring zebrafish larvae responsiveness to gradual Light-ON changes up to
167 1200lux after a period of Light-Off **(Fig 1a).** A principal component analysis (PCA) identified 11
168 swimming behavioral parameters, with PC1 and PC2 capturing over 72% and 24% of the data
169 variance, respectively**.** The total swim distance (*totaldist*) was the most influential parameter in
170 PC1 to quantify differences between MPTP-treated and untreated genotypes **(Fig. 1b)**.

171 In the VMR assay, both Panx1a$^{+/+}$ and Panx1a$^{-/-}$ larvae responded to MPTP treatment
172 (1µM to 50µM) in Light-ON conditions, with a decline in swimming distance as the MPTP dose
173 increased **(Fig. 1c).** Acute MPTP treatment consistently decreased swimming activity in both
174 Panx1a$^{+/+MPTP}$ and Panx1a$^{-/-MPTP}$ larvae compared to untreated controls, even at the lowest
175 concentration tested. The average total distance covered in a 10-second time bin was 25.6 $\pm$ 0.8
176 mm (Panx1a$^{+/+}$) and 21.1 $\pm$ 0.4 mm (Panx1a$^{-/-}$), with no statistically significant differences
177 between genotypes in the presence of MPTP. **Fig. 1d** shows that the initial Light-OFF period
178 reduced swimming distance to a baseline, followed by the resumption of swimming activity in
179 untreated larvae as light increased from 10% (400lux) to 40% (1200lux) Light-ON over the next
180 40 minutes. This result underscores the impact of Panx1a depletion and acute MPTP treatment on
181 the visuomotor response in 6dpf zebrafish larvae.

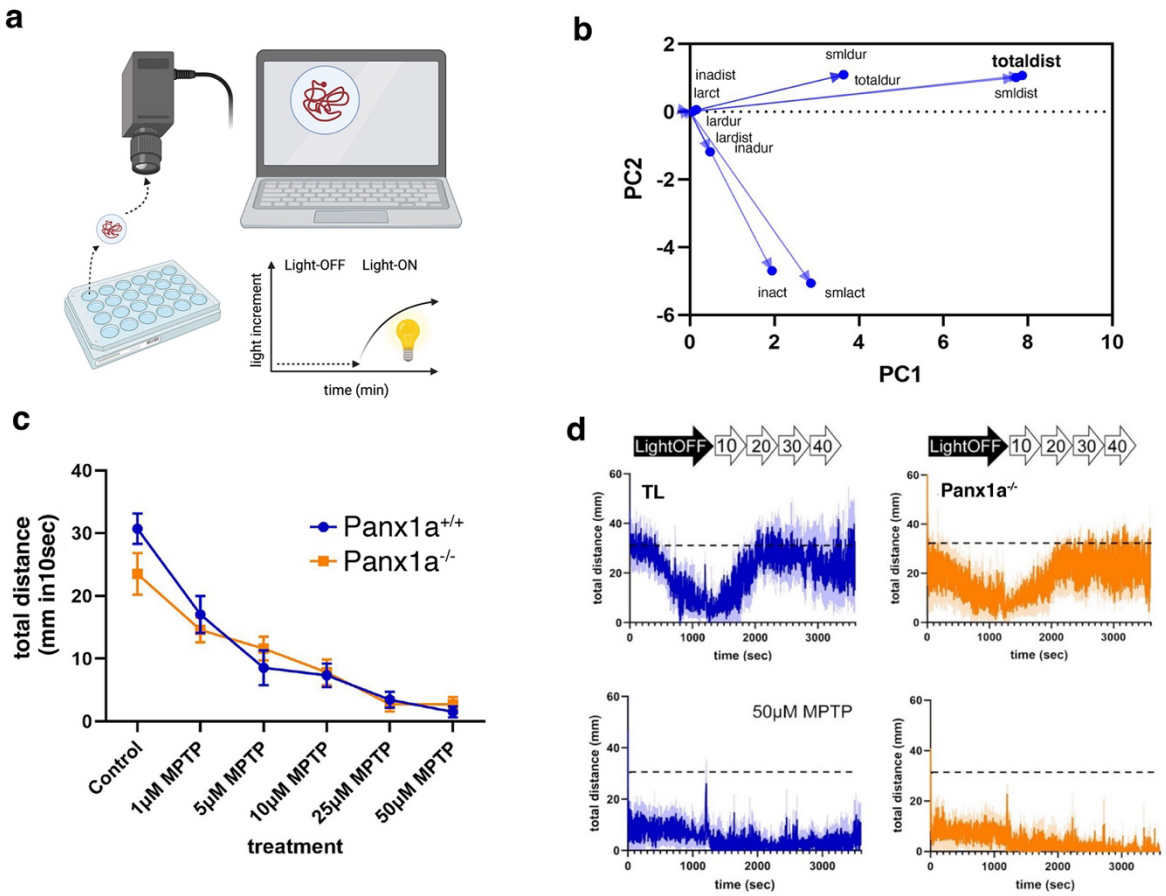

Figure 1: ***Acute treatment with MPTP alters zebrafish locomotion.*** a) Experimental setup for video recording and light stimulation of 6dpf larvae during a modified visual-motor response (VMR) assay. b) Principal Component Analysis of 11 behavioral parameters. c) Concentration-dependent impact of acute MPTP treatment on swimming behavior without (control) or after 4hrs exposure. d) Cumulative traces representing the Mean (dark blue/orange) and SEM (light blue/orange) for n=16 larvae/genotype and MPTP treatment condition. The horizontal dashed line indicates the average total swimming distance of untreated Panx1a$^{+/+}$ larvae. Statistics: Student t-test; Values represent Mean ± SEM for total distance of swimming in mm in a 10-second time-bin. The image in a) was created with BioRender.

MPTP treatment of Panx1a$^{+/+}$ and Panx1a$^{-/-}$ larvae caused transcriptional responses associated with altered mitochondrial metabolism, cell homeostasis, and cell death.

The response to MPTP exposure was characterized by transcriptional changes indicative of its neurotoxic effects. Experimental RNA-seq analysis and a computational approach aimed to

198 elucidate the transcriptional responses to acute MPTP treatment in Panx1a knockout (Panx1a$^{-/-}$
199 ^{MPTP}) and wild-type (Panx1a$^{+/+MPTP}$) larvae, unraveling key regulatory pathways underlying
200 MPTP neurotoxicity.

201 Baseline gene expression profiles of Panx1a$^{-/-}$ and Panx1a$^{+/+}$ larvae were different before
202 MPTP exposure, with n=724 genes upregulated and n=1030 genes downregulated in the
203 knockout group compared to wild-type controls **(Fig.2a)**. Following a brief exposure to MPTP (4
204 hours), both genotypes exhibited substantial alterations in gene expression patterns, highlighting
205 the dynamic nature of the cellular response to MPTP. Notably, the magnitude of gene expression
206 dysregulation was markedly amplified in Panx1a$^{-/-MPTP}$ larvae post-treatment compared to
207 Panx1a$^{+/+MPTP}$ counterparts (downregulated: Panx1a$^{+/+MPTP}$ n=3764 genes, Panx1a$^{-/-MPTP}$ n=4828
208 genes; upregulated: Panx1a-$^{+/+MPTP}$ n=3500 genes, Panx1a$^{-/-MPTP}$ n=4749 genes; false discovery
209 rate: FDR < 0.05) **(Fig. 2b,c)**.

210 To interpret the biological pathways perturbed by MPTP treatment, we conducted a gene
211 set expression analysis (GSEA) [45]. The visualization of enrichment within the top 50 Hallmarks
212 pathways provided first insights into intricate regulatory networks modulating neuronal responses
213 to MPTP exposure in the context of Panx1a ablation. Our analysis revealed significant
214 enrichment of pathways associated with metabolism and cell death, including oxidative
215 phosphorylation (Oxiphospho), glycolysis, reactive oxygen species (ROS) regulation,
216 mammalian target of rapamycin complex 1 (mTORC1) signaling, fatty acid metabolism, and
217 hypoxia. Considering the mitochondrial dysfunction in MPTP-induced neurotoxicity, the next
218 step of our investigation prioritized the analysis of how Panx1a ablation affected pathways linked
219 to mitochondrial homeostasis and their relationship to neurodegeneration.

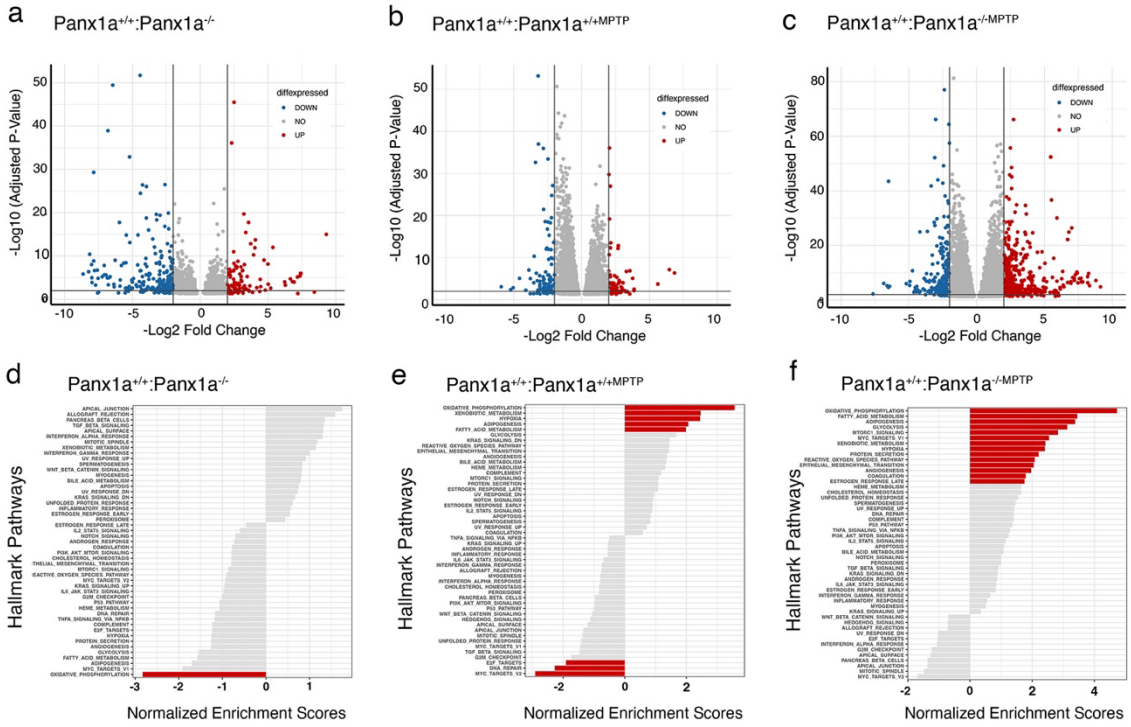

Figure 2: *MPTP treatment caused greater disruption of gene expression in Panx1a$^{-/-}$ larvae*. a-c) illustrates the log2 fold change of differentially expressed genes pre- and post-MPTP exposure, with changes exceeding a two-fold threshold highlighted in red (upregulated) or blue (downregulated). d-f) Gene set enrichment analysis (GSEA) revealing normalized enrichment scores (NES) for the top 50 ranked Hallmark pathways. Enriched pathways are denoted in red (padj <0.05), indicating significant alterations in biological processes associated with MPTP treatment in knock-out larvae compared to wild-type counterparts.

Panx1a ablation and MPTP treatment altered the differential gene expression of biomarkers for NDDs.

Panx1a ablation and MPTP treatment induce differential gene expression of biomarkers associated with NDDs. We examined gene expression patterns linked to neurodegenerative pathways, including AD, PD, ALS, and HD, by leveraging the KEGG's Pathway-based

235 Classification of Diseases database and the ZFIN database to identify zebrafish orthologs of
236 human or mouse genes annotated in KEGG.

237 The computational analysis unveiled insight into distinct differential gene expression
238 (DEG) across the selected disease categories following Panx1a ablation and MPTP treatment
239 **(Fig. 3a and Suppl. Table 1)**. The classifier *GO:Pathway to Neurodegeneration* identified 22
240 regulated genes. The downregulation of the microtubule-associated tau gene (*mapta*) stood out,
241 given its implication in neurofibrillary degeneration observed in AD and PD. In general, the
242 overlap in DEG patterns following Panx1a ablation was notable considering the distinct clinical
243 manifestations of PD, AD, ALS, and HD **(Fig. 3b-f).** A shared feature of AD, ALS, and HD
244 pathways was NMDA-receptor gene downregulation (*grin2aa, grin2ab, grin2bb*). Noteworthy
245 changes in PD included the downregulation of zebrafish variants of human alpha-Synuclein, the
246 beta- and gamma-synuclein genes (*sncb, sncg*), along with the dopamine receptor 1b (*dr1b*), the
247 Ca^{2+} calcium/calmodulin-dependent protein kinase II beta isoforms (*camk2b1, camk2b2*), and the
248 DnaJ heat shock protein family (Hsp40) member C5 (*dnaj5c*) encoding a protein with anti-
249 neurodegenerative properties. The downregulation of zebrafish orthologs (*camk2b2, camk2bl*) of
250 the murine Ca^{2+}/calmodulin dependent protein kinase II Beta, a protein found in the Panx1
251 interactome [46], showed that Panx1a loss also affected a potential protein binding partner. All
252 disease pathways genes showed an upregulation of mitochondrial electron transport chain genes
253 (*uqcr10, uqcrfs, ndufa11*), implying that mitochondrial overactivation was a shared molecular
254 hallmark. The DEG suggested that early in larval life ablation of Panx1 and acute exposure to a
255 single dose of MPTP prevented or delayed the activation of neurodegenerative pathways at the
256 cost of disturbing mitochondrial homeostasis.

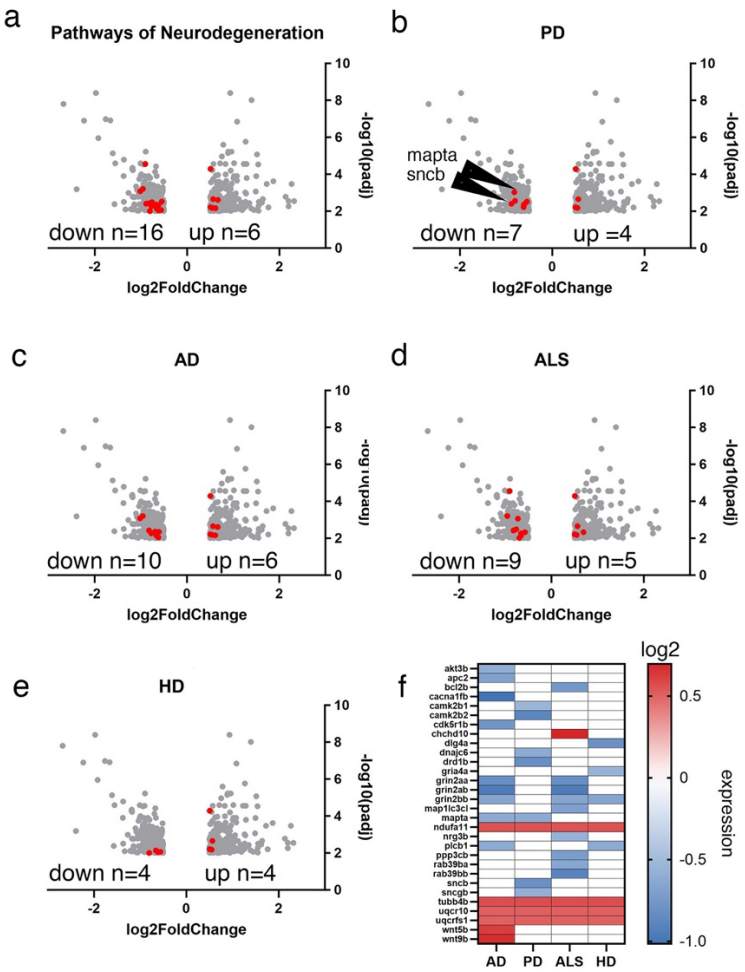

Figure 3: *Loss-of Panx1a and MPTP treatment altered the differential expression of genes in neurodegenerative pathways.* a-e) Volcano plots illustrate the differential gene expression of disease pathway genes in Panx1a$^{+/+MPTP}$ and Panx1a$^{-/-MPTP}$ larvae. The red dots represent regulated genes. Down and up refers to genes with reduced or enhanced expression in Panx1a$^{-/-}$ larvae genes (cutoff filter: log2 >0.5 or <-0.5; padj <0.01). f) Heatmap illustrating shared and distinct deregulation of the expression of genes in both genotypes. Genes in grey represent all 671 differentially expressed genes detected in both genotypes. AD, Alzheimer's disease; PD, Parkinson's disease, ALS, Amyotrophic lateral sclerosis; HD, Huntington's disease.

Panx1a ablation and MPTP treatment caused a metabolic crisis affecting biological processes related to energy metabolism, hypoxia, reactive oxygen species, and fatty acid homeostasis.

A comprehensive computational analysis, leveraging GSEA, explored the impact of MPTP treatment on Panx1a$^{+/+}$ and Panx1a$^{-/-}$ zebrafish larvae's mitochondrial health. The GSEA

272 result demonstrated an enrichment of the oxidative phosphorylation pathway in both
273 Panx1a$^{+/+MPTP}$ (n=100) and Panx1a$^{-/-MPTP}$ larvae (n=155) with a log2 fold filter set to >0.5 and <-
274 0.5 and a padj of <0.01 **(Fig. 4a)**. Only n=38 genes were different in untreated controls showing
275 that MPTP treatment impacted this pathway significantly.

276 The notable differential gene expression modulation and directionality of changes in
277 Panx1a$^{-/-MPTP}$ larvae was also found in biological processes downstream of oxidative
278 phosphorylation, such as *GO:0006096 – Glycolysis*, *GO:0001666 - Response to Hypoxia*,
279 *GO:0000302 - Response to reactive oxygen species (ROS), GO:0030968 - Unfolded Protein*
280 *Response (UPR), and GO:0006631 - Fatty acid metabolic process* **(Fig. 4d-h; Suppl. Tables 2-**
281 **6)**.

282 Notable Panx1a$^{-/-MPTP}$ specific regulations of glycolysis genes were the dysregulation of
283 two enolase genes, *eno1a/b* and *eno2*, key enzymes for cellular bioenergetics, without which
284 glycolysis cannot produce ATP, which reduces hypoxia tolerance **(Fig. 4d, Suppl. Table 2)**.
285 Likewise, the differential expression of pyruvate kinases *pkma/b*, phosphofructokinases *pfkma/b*,
286 and phosphoglycerate mutase A (*pgam1a*) demonstrate the switch to an oxygen-independent, and
287 relatively inefficient way of ATP generation when Complex I is blocked by MPTP treatment.

288 Furthermore, MPTP treatment caused the differential expression of hypoxia or ROS
289 related pathways in Panx1a$^{-/-MPTP}$ larvae that can promote neuronal cell death (*hif1al, ldha, ddit4,*
290 *egln3*) **(Fig. 4 e,f, Suppl. Tables 3,4)**. A notable change to expression in the unfolded protein
291 response (UPR) was a gene encoding for a protein, *sec13*, that functions as an activator of the
292 amino acid-sensing branch of the mTORC1 signaling pathway **(Fig. 4g; Suppl. Table 5)**. Other
293 regulated genes like *fktn, chac1, atf4a* are part of a signaling complex linked to synaptic function.
294 More specifically, the mammalian homolog of *fktn* regulates synaptic function via inhibition of
295 the ATF4 transcription factors complex with DISC1 (Disrupted-in-schizophrenia 1), or function

296 like *chac1*as a pro-apoptotic component of the unfolded protein response pathway by mediating
297 the pro-apoptotic effects of the ATF4 in the ATF4-ATF3-DDIT3/CHOP cascade.

298 The notable upregulation of *Fatty acid metabolic process* (GO:0006631) illustrated how
299 Panx1a ablation affected energy homeostasis **(Fig. 4h; Suppl. Table 6)**. For example, the
300 upregulated fatty acid elongation enzymes represented by *elovl1b, elovl4b, elovl5,* or *elovl7a/b*
301 are important for the mitochondrial fatty acid β-oxidation, the major pathway for the degradation
302 of fatty acids that is essential for maintaining energy homeostasis. The transcriptional regulation
303 of five apolipoproteins *apoea/b, apoa1a, apobb.1*, and *apoc1* signified pleiotropic effects on
304 lipoprotein metabolism. The upregulation of *apoea/b* was notable since human ortholog(s) are
305 implicated in multiple diseases, including Alzheimer's disease, artery disease, cerebrovascular
306 disease, eye disease, and familial hyperlipidemia. We reasoned that an accumulation of fatty
307 acids in mitochondria above physiological levels could have harmed mitochondrial function in
308 Panx1a$^{-/-MPTP}$ larvae causing the observed changes to hypoxia and reactive oxygen species-related
309 processes.

310 We reasoned that the altered expression of genes in the oxidative phosphorylation
311 pathway affected ATP production, with the absence of the ATP-release channel Panx1a
312 amplifying the effect of Complex I blockage by MPP+. To validate this hypothesis, we quantified
313 extracellular ATP concentrations both before and after MPTP treatment in both genotypes. The
314 impact of MPTP treatment on extracellular ATP levels was pronounced in Panx1a$^{+/+MPTP}$ larvae,
315 demonstrating a significant reduction (Panx1a$^{+/+}$: 3.12 $\pm$ 0.28 nM/µg; Panx1a$^{+/+MPTP}$: 0.96 $\pm$ 0.27
316 nM/µg; P-value=0.0011), indicating a limitation in ATP production **(Fig. 4i)**. Conversely, MPTP
317 treatment had a minor effect on Panx1a$^{-/-MPTP}$ larvae, revealing a decrease of low ATP levels
318 (Panx1a$^{-/-}$: 1.73 $\pm$ 0.31 nM/µg; Panx1a$^{-/-MPTP}$: 0.95 $\pm$ 0.15 nM/µg; P-value=0.044).

In summary, the identified molecular and biochemical changes after short-term MPTP treatment demonstrate that the depletion of extracellular ATP after inhibition of Complex I triggered the differential expression of specific pathways that sense and respond to the metabolic crisis.

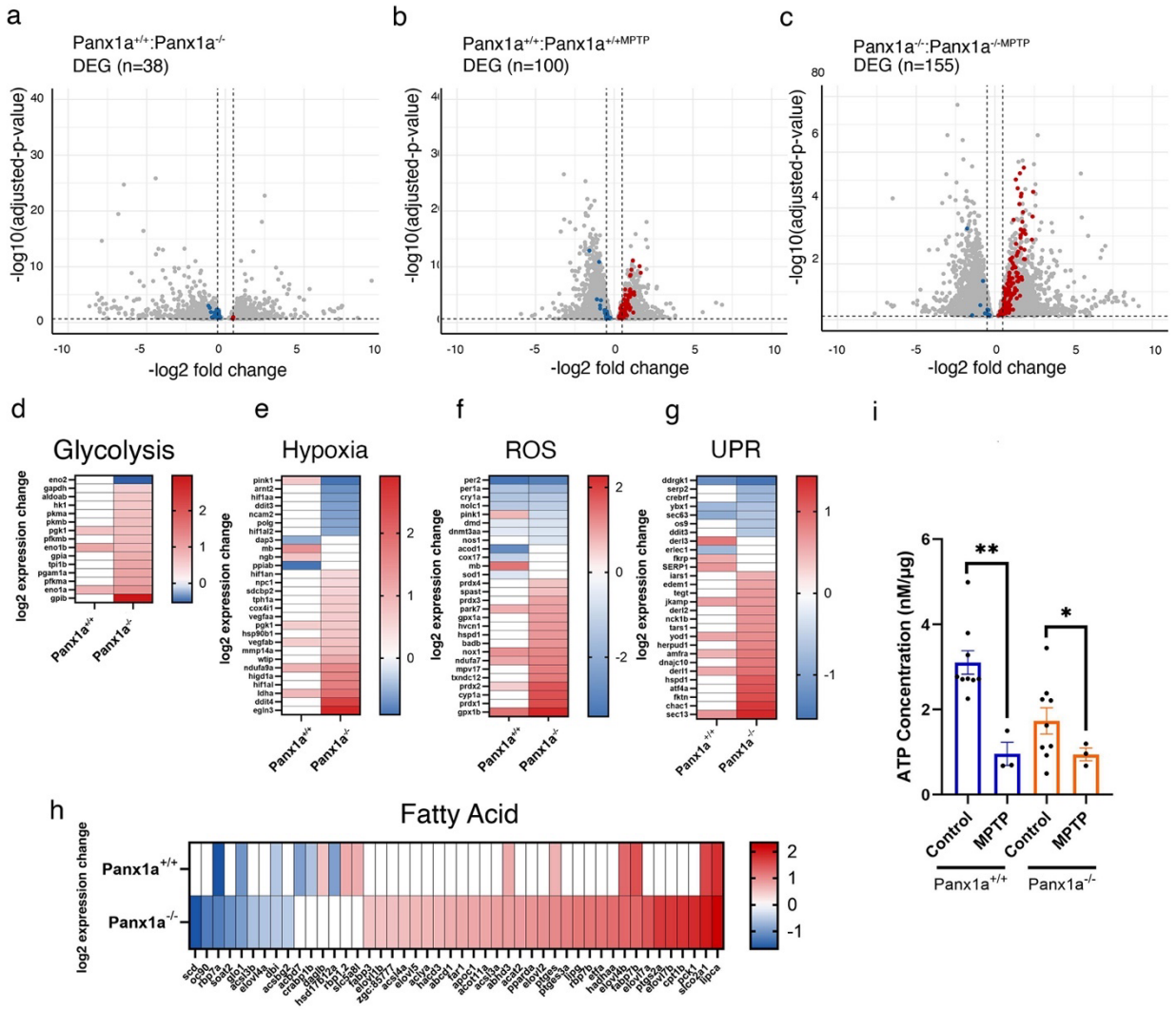

Figure 4: *Acute treatment with MPTP caused a metabolic crisis and reduced ATP release in Panx1a$^{+/+}$ larvae*. a-c) Differentially expressed genes in the oxidative phosphorylation pathway. Dots in blue and red represent significantly regulated genes in the oxidative phosphorylation

329 pathway. Grey dots represent all DEGs. d-h) Heatmaps illustrate the differential expression of
330 genes identified in the biological processes: GO:0006096 – Glycolysis, GO:0001666 - Response
331 to Hypoxia, GO:0000302 - Response to reactive oxygen species (ROS), GO:0030968 - Unfolded
332 Protein Response (UPR), and GO:0006631 - Fatty acid metabolic process. i) ATP concentrations
333 were measured before and after acute MPTP treatment. MPTP treatment caused a significant
334 downregulation in Panx1a$^{+/+MPTP}$ larvae (P-value < 0.05). No significant differences in ATP
335 concentrations were observed in Panx1a$^{-/-MPTP}$ larvae. The ATP concentrations were adjusted for
336 protein concentration to evaluate extracellular ATP levels across multiple samples. Each sample
337 represented a pool of 50 6dpf larvae. Statistical approach: Welch's t-test. The number of
338 experimental replicates: Panx1a$^{+/+}$ and Panx1a$^{-/-}$ untreated controls n=9; MPTP treatment
339 conditions n=3. Mean ± SEM. Statistical significance was indicated as *: P-value * <0.05, ns =
340 not significant.
341
342
343
344 ***Loss of Panx1a promotes cell death in the acute MPTP model.***

345 The investigation into the role of Panx1a in cell death was prompted by the anticipated
346 consequences of altered mitochondrial metabolism, ROS, Hypoxia and the UPR. The enrichment
347 of genes in the mTORC1 pathway, identified through GSEA (see Fig. 2), implied disturbances in
348 mTOR signaling, which could impact various pathways including glucose metabolism, energy
349 production, mitochondrial function, cell growth, and autophagy. The differential gene expression
350 of mTORC1 pathway genes in untreated controls (n=13), Panx1$^{+/+MPTP}$ (n= 74), and Panx1a$^{-/-MPTP}$
351 larvae (n=121) exhibited an enrichment trend that showed that Panx1a$^{-/-MPTP}$ were affected most
352 by the mitochondria dysfunction **(Fig. 5a-c)**.

353 In Panx1a$^{-/-MPTP}$ larvae, notable groups of genes upregulated in the mTOR pathway
354 included ten Wnt/frizzled genes (*wnt5a, wnt7aa, wnt9a/b, wnt10a, wnt11, fdz4, fdz6, fdz7a/b*)
355 with known roles in early apoptosis stages. Additionally, the upregulation of eight subunits of
356 vacuolar ATPases (*V-ATPase; atp6v1aa atp6v1ab atp6v1b2, atp6v1g1 atp6v1h atp6v1c1b*
357 *atp6v1ba atp6v1f*) implicated a disruption of cellular homeostasis. Furthermore, late
358 endosomal/lysosomal adaptor and MAPK and mTOR activator genes (LAMTOR/Ragulator)
359 encoding scaffold proteins forming complexes that regulate multiprotein signaling units on late
360 endosomes/lysosomes were involved in acidification (*lamtor2, lamtor3, lamtor5*).

361 Other functional enrichment analyses showed differentially expressed genes associated
362 with cell death (GO:0008219), autophagy (GO:0006914), and the execution phase of apoptosis
363 (GO:0097194). In Panx1a$^{-/-MPTP}$ larvae, 223 cell death-related genes were identified, while
364 Panx1a$^{+/+MPTP}$ larvae exhibited regulation in 107 genes **(Fig 5d, Suppl Table 7)**. The analysis of
365 autophagy genes mirrored the overall pattern of cell death, with a substantial six to eleven-fold
366 increase in differentially expressed genes when comparing untreated with MPTP-treated larvae
367 (Panx1a$^{+/+MPTP}$, n=38; Panx1a$^{-/-MPTP}$, n=70) **(Fig. 5e)**. The unique molecular response in the
368 absence of Panx1a was evident, with Panx1a$^{-/-MPTP}$ larvae showing a notable increase in
369 differentially upregulated (n=35) and downregulated genes (n=16) **(Suppl Table 8)**. Among the
370 upregulated genes, transmembrane 41b (*tmem41b*), tumor protein p53-inducible nuclear protein 1
371 (*tp53inp1*), and the stimulator of interferon (*sting1*), pointed towards the activation of autophagy
372 and cellular stress response. These genes play essential roles in autophagosome biogenesis, pro-
373 apoptotic responses, and inflammation mediation, respectively, contributing to cellular
374 adaptations and responses under MPTP-induced conditions.

375 Activation of the execution phase of apoptosis was observed in Panx1a$^{-/-MPTP}$ larvae, as
376 demonstrated by the upregulation of seven members of the caspase gene family, including
377 initiators of apoptosis *casp9* and *casp20*, and executioner phase caspases *casp3a, casp6a,*
378 *casp6b1*, and *casp7*. The log2 fold ratio = 7.15 upregulation of the inflammatory caspase *caspbl*
379 (alternative name casp19b) was particularly notable as a hallmark for the execution phase of
380 apoptosis, downstream of the assembly of the inflammasome complex, leading to the cleavage
381 and activation of the proinflammatory cytokine *il1b* **(Fig. 5f, Suppl Table 9)**.

382 To assess cell death, an *in-vivo* cell death stain, acridine orange (AO), was utilized **(Fig.**
383 **5g)**. Notably, AO-stained nuclei were particularly prominent in brain regions known for
384 dopaminergic neuron expression or the optic tectum, which receives inputs from hypothalamic

385 dopaminergic neurons. In the absence of treatment, Panx1a$^{+/+}$ larvae exhibited the lowest number
386 of dead cells (Panx1a$^{+/+}$ = 39.67, Panx1a$^{-/-}$ = 66). The number of AO-positive cells in Panx1a$^{-/-}$
387 larvae was significantly higher compared to Panx1a$^{+/+}$ (P-value = 0.0056) **(Fig. 5h)**. MPTP
388 treatment increased cell death in both genotypes (P-value = 0.0130), with an average of n=174
389 AO-positive cells in Panx1a$^{-/-}$MPTP and n=125 in Panx1a$^{+/+MPTP}$ larvae.

390 In summary, the results underscore a multifaceted role for Panx1a in modulating gene
391 expression related to cell death, apoptosis, and autophagy. Imaging of cell death *in vivo*
392 implicates regions with loss of dopaminergic neurons.

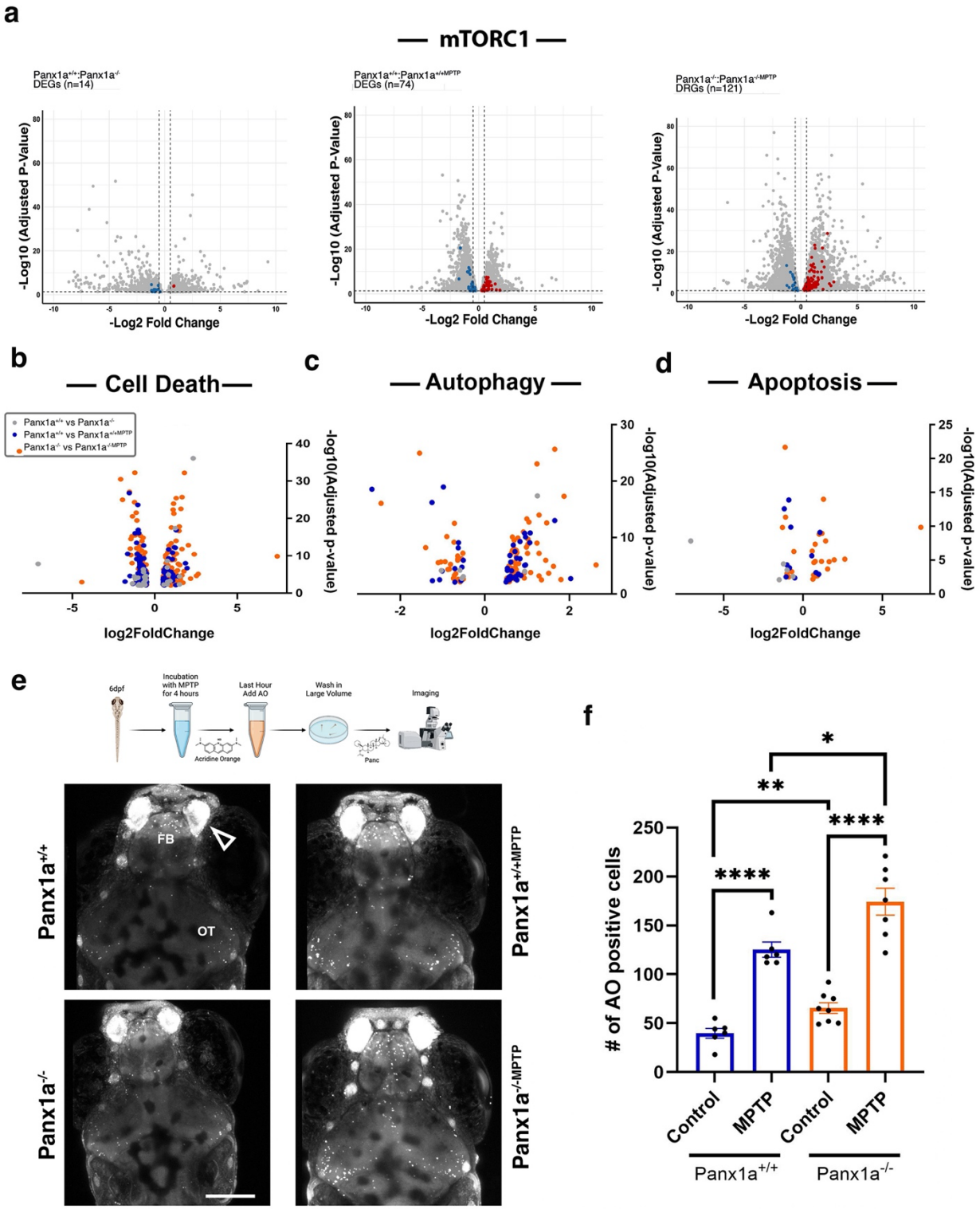
a
mTORC1
Panx1a+/+:Panx1a-/- DEGs (n=14)
Panx1a+/+:Panx1a+/+MPTP DEGs (n=74)
Panx1a-/-:Panx1a-/-MPTP DRGs (n=121)
-Log10 (Adjusted P-Value)
-Log2 Fold Change
b
Cell Death
c
Autophagy
d
Apoptosis
Panx1a+/+ vs Panx1a-/-
Panx1a+/+ vs Panx1a+/+MPTP
Panx1a-/- vs Panx1a-/-MPTP
-log10(Adjusted p-value)
log2FoldChange
e
6dpf
Incubation with MPTP for 4 hours
Last Hour Add AO
Wash in Large Volume
Imaging
Acridine Orange
Panc
FB
OT
Panx1a+/+
Panx1a+/+MPTP
Panx1a-/-
Panx1a-/-MPTP
f
# of AO positive cells
Control
MPTP
Control
MPTP
Panx1a+/+
Panx1a-/-

393

394

395 **Figure 5:** *Loss of Panx1a promotes cell death in the acute MPTP model.* a) Differentially
396 regulated genes in the mTORC1 pathway. Blue and red dots represent regulated genes in the
397 pathway. Grey dots represent all DEGs. b-d) Significantly regulated genes (padj ≤ 0.01) were
398 compared against zfin lists of cell death, apoptosis, and autophagy. Regulated genes were plotted.
399 e) Experimental outline of the *in-vivo* cell death assay. Representative projection views of Z-
400 stacks representing a depth ≈ 100µm collected from untreated and MPTP-treated Panx1a$^{+/+}$ and
401 Panx1a$^{-/-}$ larvae. f) Quantification of acridine-orange positive cells. Statistical approach:
402 Significance was calculated using an unpaired t-test. Number of larvae, n=7 for all treatments.
403 Mean ± SEM. Statistical significance was indicated as *: P-values * <0.05, ** <0.01, *** <0.005,
404 **** <0.001.
405

406

407 ***Panx1a ablation and MPTP treatment altered neurotransmitter receptors and the ion***

408 ***homeostasis of chemical synapses.***

409 A computational DESeq2 analysis of the RNA sequencing analysis, employing a log2

410 gene filter of >0.5 and <-0.5 with a padj < 0.01, revealed 681 differentially expressed genes in

411 Panx1$^{-/-MPTP}$ and Panx1$^{+/+MPTP}$ larvae. Among these genes, 267 were upregulated and 414 were

412 downregulated in both genotypes. Functional enrichment analysis, utilizing curated gene lists

413 from public repositories such as ZFIN.org and KEGG, along with Gene Ontology search terms,

414 delineated specific alterations in ion homeostasis and neurotransmitter receptors at chemical

415 synapses **(Fig 6)**.

416 The analysis of the Gene Ontology search terms *GO:Biological Process* and *GO:Cellular*

417 *Compartment* indicated significant upregulation of biosynthetic pathways, suggestive of

418 increased metabolic activities in 6dpf larvae with Panx1a ablation **(Fig. 6a,b)**. Conversely,

419 downregulated genes were enriched for biological processes related to neurotransmission at

420 chemical synapses, synaptic signaling, and neurodevelopment, affecting both pre- and

421 postsynaptic compartments. Specifically, the query term *GO:0045202 – Synapse* identified 53

422 downregulated genes and no upregulated genes, while the terms *GO:0098793 – Presynapse* and

423 *GO:0098794 – Postsynapse* identified 35 and 36 differentially expressed genes, respectively
424 **(Fig. 6c,d; Suppl Table 10)**.
425 STRING analysis of the downregulated genes demonstrated a significant impact of
426 Panx1a ablation on GABAergic and glutamatergic transmission. Notably, ligand-gated and G
427 protein-coupled GABA receptor subtypes *(gabra6b, gabrb1, gabrb3, gabrb4, gabrz, gabrg2,*
428 *gabrr2a)* (**Cluster I)**, ionotropic NMDA (*grin2aa, grin2ab, grin2bb*), AMPA (*gria4a*), and
429 kainite receptors (*grik2*) were downregulated alongside other regulators of synaptic plasticity
430 (**Cluster II Suppl. Fig. 1**). For example, the mouse ortholog of *shisa9a* is a regulator of short-
431 term neuronal synaptic plasticity in the dentate gyrus associated with AMPA receptor function.
432 Likewise, the discs large MAGUK scaffold protein genes *dlg2* (PSD93) and *dlg4* (PSD95) were
433 downregulated.
434 **Cluster III** encompassed genes encoding pre-synaptic proteins with essential roles in
435 neurotransmitter release via the formation of the SNARE complex (synaptosomal-associated
436 protein: *snap25a, snap25b*), calcium dynamics in response to depolarization, or vesicle
437 exocytosis (synaptotagmin: *syt1a, syt5b*; syntaxin: *stx1b, stx12l, stxbp1a*; complexin; *cplx2,*
438 *cplx2l, cplx3b, cplx4a*). The presynaptic downregulation of glutamate decarboxylase gene 2
439 (*gad2*) expression is notable; the Gad2 protein catalyzes the presynaptic production of GABA,
440 which suggests a negative feedback loop as downregulation of GABA production corresponds
441 with reduced GABA receptor expression.
442 Furthermore, deregulation of inorganic ion transporters (n=45) and calcium binding
443 proteins (n=27) was observed in Panx1a$^{-/-MPTP}$ larvae **(Fig. 6d).** Synaptically localized anionic ion
444 transporters (n=15) with reduced expression in the nervous system **(Suppl. Fig 1, Clusters I, II)**
445 included AMPA and NMDA receptors, or chloride permeable GABA receptors. The four up-
446 regulated genes included a Na-Cl cotransporter-like protein (*slc12a10.2*), an anion:anion

447 antiporter with bicarbonate transmembrane transporter activity (*slc4a1b*), or a gene encoding a
448 voltage-gated chloride channel (*clcn2c*) that maintains chloride ion homeostasis. Deregulation of
449 cation transporters (n=25) included transporters and channels permeable for potassium (*kcna1b,*
450 *kcnip1b, kcnip3b, kcn1a.1, kcnk3b*), calcium (*cacna1fb, cacna1ha*), sodium (*scn3b*), or co-
451 transporters for sodium and chloride (*slc12a10.2*), symporters for potassium and chloride
452 (*slc12a5b*), a potassium-dependent sodium/calcium exchanger (*slc24a5*), or a
453 GABA:sodium:chloride symporter (*slc6a1a*). The loss of Panx1a also affected the differential
454 expression of calcium-binding proteins (n=26). Notable examples include members of the
455 protocadherin gene family (*pcdh1a, pcdh8. Pcdh17, pcdh19*) regulating neurotransmission and
456 synaptic plasticity.

457 Overall, the computational analysis suggested that Panx1a ablation, in conjunction with
458 MPTP treatment, perturbed ion homeostasis and neurotransmitter release at synapses, affecting
459 neurotransmission and synaptic plasticity across pre- and postsynaptic compartments.

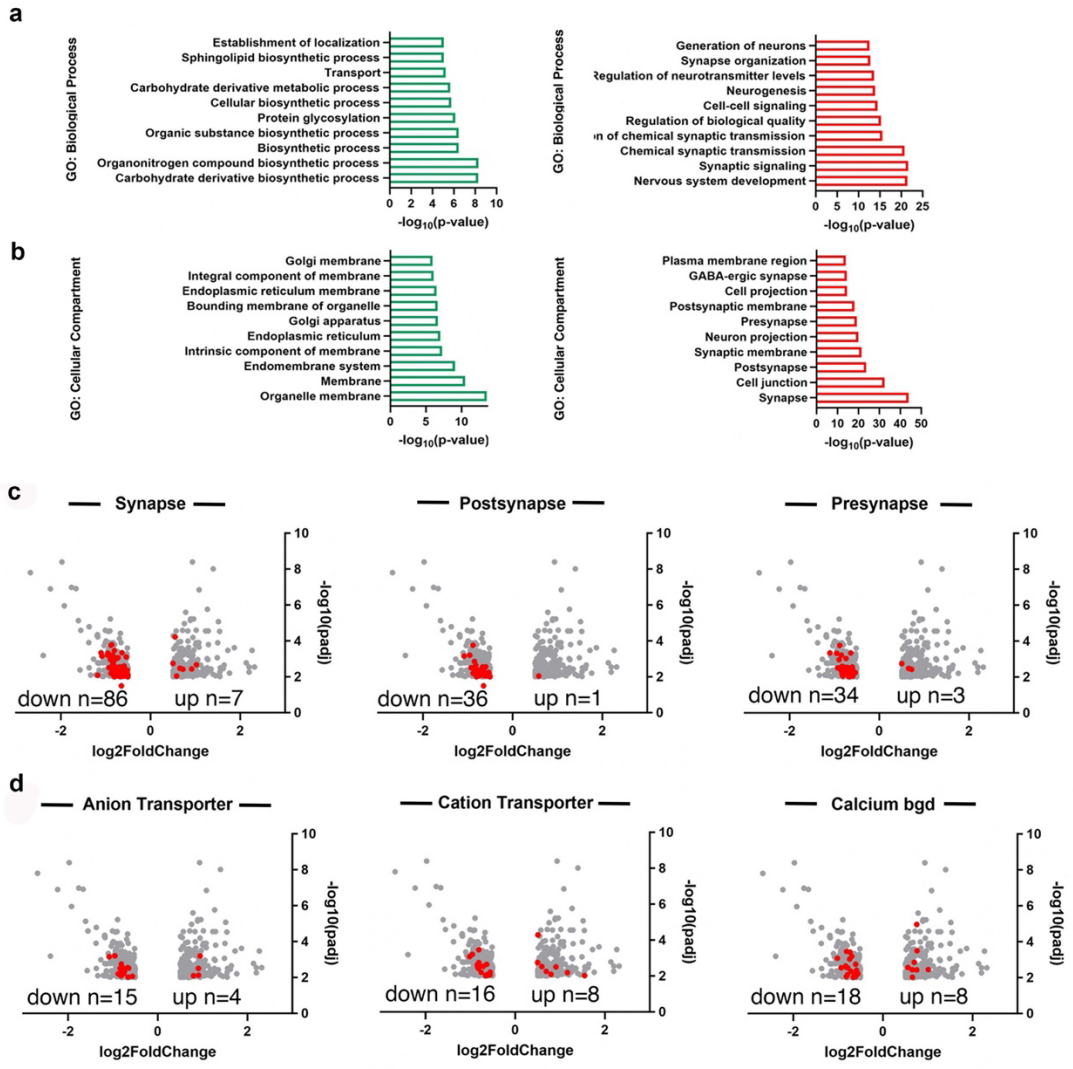

Figure 6: *Loss-of Panx1a and MPTP treatment altered the differential expression of genes localized in chemical synapses.* a,b) Summary of the ten most enriched Gene Ontology Biological Processes and Cellular compartments found in Panx1a$^{+/+MPTP}$ and Panx1a$^{-/-MPTP}$ treated larvae. The P-values of each category represent the false discovery rate presented as inverse log10. c), d) Volcano plots represent the differentially expressed genes in Panx1a$^{+/+MPTP}$ and Panx1a$^{-/-MPTP}$ treated larvae (red dots). Gray dots represent the 671 differentially expressed genes found in both genotypes. The cutoff filter was: log2 >0.5 or <-0,5 and padj <0.01.

Loss-of-Panx1a function alters the power of theta, beta- and gamma-waves in the optic tectum.

The impact of MPTP-induced cell death and alterations in energy metabolism on brain activity, was assessed Local Field Potential (LFP) recordings. Our focus was on determining whether the

473 absence of Panx1a influenced local neuronal circuits following acute MPTP treatment. We
474 strategically positioned electrodes in the optic tectum (OT) and lateral dorsomedial forebrain
475 (DM), regions previously identified as having cell loss after exposure to 10μM MPTP **(Fig. 7a).**
476 Simultaneous recordings of brain waves were performed on awake, immobilized 6dpf
477 larvae. We categorized frequency spectra into specific bands (Theta: 3.5-7.5Hz, Beta: 12-30Hz,
478 Gamma: 35-45Hz), employing a common approach used in mammalian electrophysiological data
479 analysis that is applicable to zebrafish. Raw traces **(Fig. 7b)** underwent lowpass filtering
480 (<300Hz) to isolate Theta, Beta, and Gamma waves **(Fig. 7c,d).** Our LFP analysis focused on
481 computing Power Spectra Densities (PSDs) at these frequencies, with ranges selected from
482 human brain wave investigation.
483 Significant inverse relationships were observed for theta, beta, and gamma power in the
484 OTs of both genotypes (PSD % values: Theta - Panx1a$^{+/+}$ 0.253 vs Panx1a$^{+/+MPTP}$: 0.019, P-value
485 < 0.0001, Panx1a$^{-/-}$: 0.196 vs Panx1a$^{-/-MPTP}$: 0.275, P-value = 0.0052; Beta - Panx1a$^{+/+}$: 0.018 vs
486 Panx1a$^{+/+MPTP}$: 0.011, P-value < 0.0001, Panx1a$^{-/-}$: 0.009 vs Panx1a$^{-/-MPTP}$: 0.024, P-value <
487 0.0001; Gamma - Panx1a$^{+/+}$: 0.227 vs Panx1a$^{+/+MPTP}$: 0.397, P-value = 0.0012, Panx1a$^{-/-}$: 0.145 vs
488 Panx1a$^{-/-MPTP}$: 0.131, P-value = 0.849). Similar trends were observed in the DM following MPTP
489 treatment in both genotypes. PSDs of Panx1a$^{+/+}$ and Panx1$^{-/-}$ larvae either decreased in Panx1a$^{+/+}$
490 (Theta: Panx1a$^{+/+}$: 0.339 vs Panx1a$^{+/+MPTP}$: 0.157, P-value < 0.0001, Panx1a$^{-/-}$: 0.330 vs Panx1a$^{-/-}$
491 ^{MPTP}: 0.231, P-value = 0.188), remained unchanged (Beta: Panx1a$^{+/+}$: 0.016 vs Panx1a$^{+/+MPTP}$:
492 0.015, P-value = 0.660, Panx1a$^{-/-}$: 0.013 vs Panx1a$^{-/-MPTP}$: 0.014, P-value = 0.978), or decreased
493 in Panx1a$^{+/+}$ and increased in Panx1a$^{-/-}$ (Gamma: Panx1a$^{+/+}$: 0.407 vs Panx1a$^{+/+MPTP}$: 0.267, P-
494 value = 0.0465, Panx1a$^{-/-}$: 0.101 vs Panx1a$^{-/-MPTP}$: 0.264, P-value < 0.0001) **(Fig. 7e,f).**
495 We demonstrated that the LFPs in neuronal circuits in the OT and DM regions responded
496 differently to MPTP+ when Panx1a was present. It was concluded that the changes occurring

within selected spectral frequency bands connect functions of Panx1 to synaptic plasticity and mammalian CNS circuit pathophysiology.

Our findings demonstrate differential responses in LFPs within neuronal circuits of the OT and DM regions to MPTP when Panx1a is present. The observed changes in selected spectral frequency bands suggest a connection between Panx1 functions and synaptic plasticity, shedding light on mammalian CNS circuit pathophysiology.

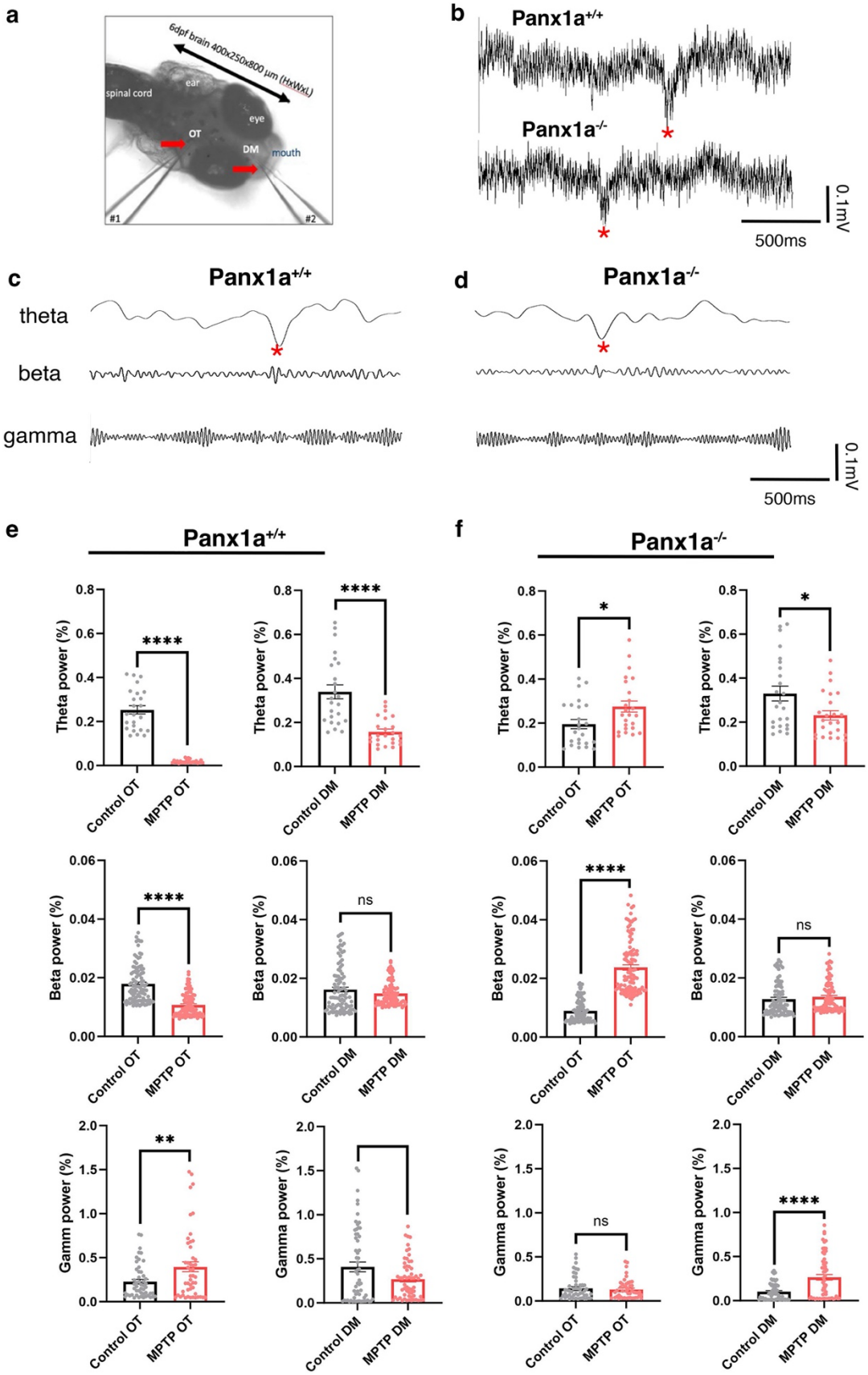
a
6dpf brain 400x250x800 µm (HxWxL)
spinal cord
ear
eye
OT
DM
mouth
#1
#2
b
Panx1a+/+
Panx1a-/-
0.1mV
500ms
c
Panx1a+/+
theta
beta
gamma
d
Panx1a-/-
0.1mV
500ms
e
Panx1a+/+
f
Panx1a-/-
Theta power (%)
Beta power (%)
Gamm power (%)
Gamma power (%)
Control OT
MPTP OT
Control DM
MPTP DM
****
*
ns
**

504

Figure 7: *Loss-of-Panx1a function alters the power of theta, beta- and gamma-waves in the optic tectum. a)* Representative image of a two-electrode setup with electrode #1 and electrode#2 placed into the optic tectum (OT) and dorsomedial forebrain (DM), respectively. b) Raw recording traces before isolating c,d) theta (3.5 – 7Hz), beta (12 -30Hz), and low gamma-wave (35 – 45Hz) frequency ranges. The red star indicates a reference point in the traces. e,f) Comparisons of the theta, beta, and gamma-power of Panx1a$^{+/+}$ and Panx1a$^{-/-}$ larvae without (control) and with 10µM MPTP treatment. Statistical approach: Outliers were removed using a ROUT test (Q = 1%). Significance was calculated using a Welch's t-test. Number of larvae, n = 8 for Panx1a$^{+/+}$ and Panx1a$^{-/-}$. Mean ± SEM. Statistical significance was indicated as *: P-values * <0.05, ** <0.01, *** <0.005, **** <0.001, ns = not significant.

Loss-of-Panx1a reverses the coherence of local field potentials.

A coherence analysis of LFPs in the frequency range from 0 to 60hz tested the impact of Panx1a ablation and MPTP treatment on the connectivity between the optic tectum (OT) and lateral dorsomedial forebrain (DM), two pivotal regions in the ascending visual pathway **(Fig. 8a).** The zebrafish ascending visual pathway comprises polysynaptic connections, with retinal input to the OT and subsequent projections from the OT to the lateral preglomerular complex and the pallium, including the DM [47,48].

MPTP treatment caused a reduction in coherence between OT and DM in Panx1a$^{+/+}$ larvae across theta (Panx1a$^{+/+}$: 0.764, Panx1a$^{+/+MPTP}$: 0.470, P-value < 0.0001) and beta frequencies (Panx1a$^{+/+}$: 0.650, Panx1a$^{+/+MPTP}$: 0.425, P-value < 0.0001) **(Fig. 8b,c)**. Panx1a$^{-/-}$ larvae exhibited the converse effect, with augmented coherence in theta (Panx1a$^{-/-}$: 0.523, Panx1a$^{-/-MPTP}$: 0.469, P-value < 0.0001) and beta frequencies (Panx1a$^{-/-}$: 0.330, Panx1a$^{-/-MPTP}$: 0.490, P-value < 0.0001). Prior investigations have associated elevated beta frequency coherence with Parkinson's disease pathology [49]. The potential ramifications of the observed beta frequency coherence increase in Panx1a$^{-/-}$ larvae warranted further exploration. Furthermore, Panx1a$^{+/+}$ larvae demonstrated a

533 notable increase in low gamma coherence (Panx1a$^{+/+}$: 0.525, Panx1a$^{+/+MPTP}$: 0.612, P-value
534 0.0001), a phenomenon previously linked to uncertainty [50].

535 Collectively, alterations in theta, beta, and low gamma coherence in Panx1a$^{+/+}$ larvae
536 suggested that MPTP treatment induced a functional modulation of neural network mechanisms,
537 likely involving a combination of loss of cell homeostasis, synaptic plasticity, and cell death.

538

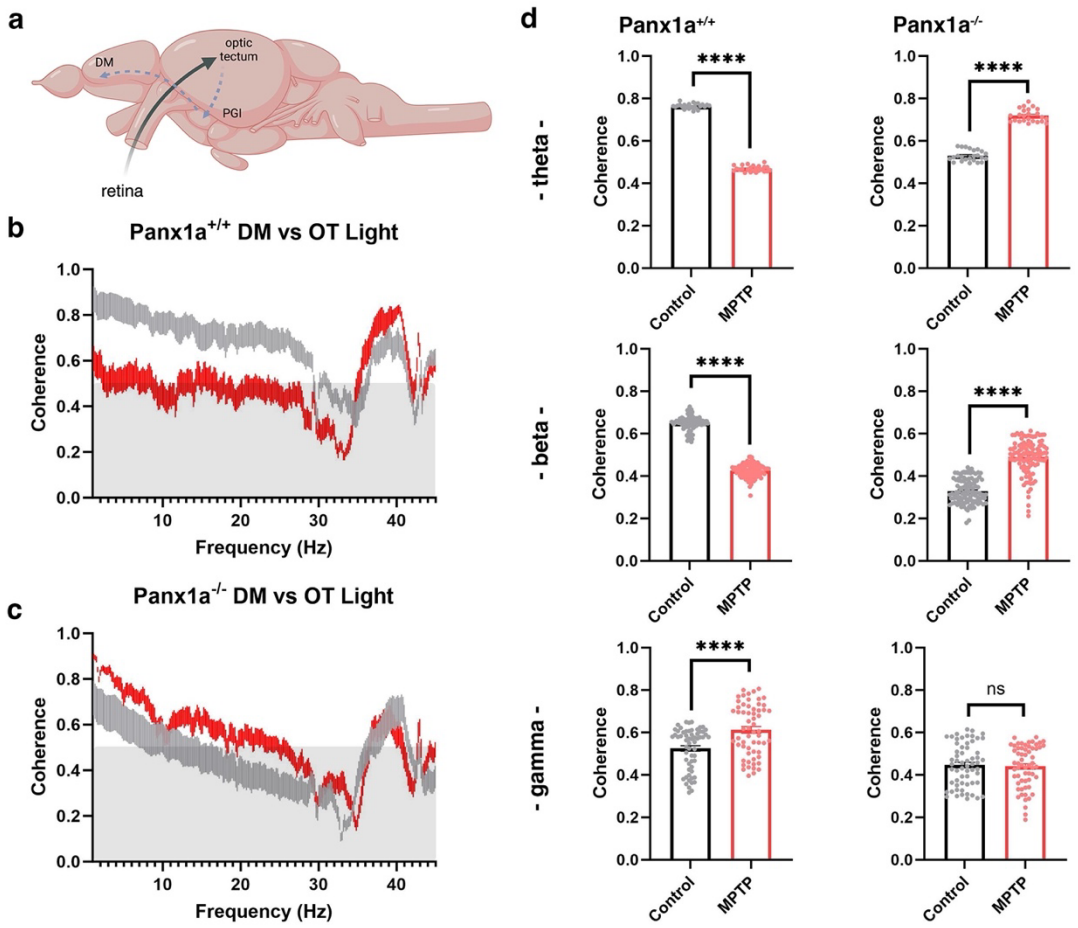

539

540

541 **Figure 8.** *Loss-of-Panx1a function reverses the coherence of local field potentials.*
542a) Outline of the ascending visual pathway. b,c) Shows the coherence of local field potentials
543 measured in the optic tectum (OT) and the dorso-medial forebrain (DM) of 6dpf Panx1a$^{+/+}$ and
544 Panx1a$^{-/-}$ larvae. The traces represent the 95% confidence intervals (CI) without (in grey) and
545 after 4hrs of treatment with 50µM MPTP (in red). d) The theta (3.5 – 7Hz), beta (12 -30Hz) and
546 gamma-waves (35 – 45Hz) coherence without (control, in grey) and after MPTP treatment (in

red). Statistical approach: Outliers were removed using a ROUT test (Q = 1%). Significance was calculated using a Welch's t-test. Number of larvae, n = 8 for Panx1a$^{+/+}$ and Panx1a$^{-/-}$. Mean ± SEM. Statistical significance was indicated as *: P-values * <0.05, ** <0.01, ***<0.005, **** < 0.001, ns= not significant.

Discussion

In this study acute MPTP treatment of 6dpf larvae served as a model to study the role of Panx1 in a period of zebrafish neurodevelopment that is considered to resemble late-term to birth in Mammalia. Perturbation of this developmental period is considered correlated with the onset of diverse neuropathological outcomes including sensory and motor deficits or learning disabilities found in neurodegenerative disorders. The principal results of this study introduce a new perspective on the role of Panx1a channels in the context of acute MPTP-induced changes of mitochondrial health; the evidence supports functions of Panx1a akin to a rheostat, regulating cell death, synapse function, and mitochondrial homeostasis.

Panx1a alters pathways to neurodegeneration.

Utilizing computational approaches, we identified an intricate interplay between Panx1a and neurodegenerative pathways following exposure to MPTP, a neurotoxin commonly employed in Parkinson's disease (PD) models. The analysis reveals compelling associations with PD and other neurodegenerative disorders, including Alzheimer's disease (AD), Amyotrophic lateral sclerosis (ALS), and Huntington's Disease (HD), thus highlighting the broad impact of Panx1a dysregulation on neuronal health. Specifically, the biomarker deregulation was consistent with Panx1a functioning as a molecular hub for signaling pathways integrating synaptic plasticity, cellular homeostasis, and mitochondrial health.

Panx1a$^{-/-MPTP}$ larvae showed a notable downregulation of beta-synuclein (*sncb*) and gamma1-synuclein (*sncgb*) genes. Zebrafish lack the expression of alpha-synuclein, a molecular

574 hallmark of PD, but express three synuclein genes known as the *sncb*, *sncga*, and *sncgb* in
575 catecholaminergic neurons throughout the CNS [51,52]. *Sncb* and *sncg* gene ablation in zebrafish
576 caused a significant reduction in motor activity and lowered the level of dopamine in the brain,
577 indicating that zebrafish synuclein proteins are required for movement regulation and dopamine
578 homeostasis [53]. In humans, ß-synuclein downregulation has been correlated with the clinical
579 phenotype and neuropathological diagnosis of a specific molecular subtype of dementia with
580 Lewy bodies, characterized by a strong decrease of β-synuclein in the frontal and temporal
581 cortices [54]. The morphological substrate, i.e. α-synuclein-immunoreactive Lewy bodies, and
582 Lewy neurites, is the same in both Parkinson's disease with dementia and Lewy body dementia.
583 Furthermore, our investigation unveiled a significant reduction in the expression of
584 microtubule-associated protein tau (*mapta*), a hallmark of AD pathology, in Panx1a$^{-/-MPTP}$ larvae.
585 This finding suggests a disruption in axonal transport processes [55,56], implicating Panx1a in the
586 maintenance of cytoskeletal integrity crucial for neuronal function. Interestingly, the number of
587 known human pathologies involving deregulated Tau expression/metabolism is increasing [57]. In
588 addition to Tau aggregation and hyperphosphorylation, Tau deregulation can occur at the
589 expression and/or splicing levels, with downregulation found in AD patients [58]. In the adult
590 zebrafish the deregulation of Tau is affected by hypoxia, promoting neuronal dysfunction and
591 degeneration [59]. The hypoxia pathway is intensified in Panx1a$^{-/-MPTP}$ larvae.
592 The bidirectional regulation of biomarkers for AD or PD includes the upregulation of
593 Wnt/ß-catenin pathway genes, tubulin, and mitochondrial genes. The dysregulation of Wnt and
594 tubulin genes is most likely a molecular fingerprint for dysfunctional synapses; canonical and
595 non-canonical Wnt pathways need to be well balanced to ensure adequate synapse numbers and
596 changes. Moreover, activation of Wnt/β-catenin signaling inhibits amyloid-β production and tau
597 protein hyperphosphorylation, and restoring Wnt/β-catenin signaling in AD represents a unique

598 opportunity for the rational design of novel therapies [60]. Interestingly, ß-catenin is an interaction
599 partner of Panx1 in human melanoma cell lines [61].

600 The upregulation of mitochondrial Complex I and Complex III genes, NADH:ubiquinone
601 oxidoreductase subunit A11 (*ndufa11*), or ubiquinol-cytochrome c oxidoreductases (*uqcr10,*
602 *uqcrfs1*), illustrate changes to mitochondrial energy metabolism and homeostasis which are
603 amplified in Panx1a$^{-/-MPTP}$ larvae. The augmented upregulation of pathways leading to hypoxia,
604 ROS-production, or the unfolded protein response further substantiate that Panx1a expression is
605 required to maintain metabolic and energetic homeostasis *in vivo*.

606 In summary, the computational analysis identified molecular indicators suggesting that in
607 metabolically challenged Panx1a-deficient larvae a cascade of pathological events unfolds that
608 makes the initiation of pathways to major neurodegenerative disorders less likely. However,
609 targeting Panx1a may result in offsetting alterations in synaptic composition and compromised
610 ATP production, accentuating thecritical roles of Panx1a in preserving neuronal viability and
611 function.

612

613 ***Panx1a alters the molecular composition and function of synapses.***

614 The observed deregulation of genes with pre- and postsynaptic localization in metabolically
615 challenged zebrafish provides new information about how Panx1 is involved in transsynaptic
616 activities and synapse organization. We link behavioral and electrophysiological deficits with
617 molecular changes at synapses that include the downregulation of excitatory ionotropic AMPA-,
618 NMDA-, and kainite receptors subunits, and the inhibitory GABA-gated chloride ion channel
619 Gabra6a, or to anion and cation channels. The differential expression of both pre- and postsynaptic
620 genes showcases transsynaptic effects of Panx1 ablation that support roles of Panx1 channels as a
621 molecular hub integrating neurotransmission and ion homeostasis.

622 In 2007, we postulated that Panx1 channel localization in postsynaptic contacts of mouse
623 cerebral cortex and the hippocampus represents a strategic position for synapse function
624 modulation [62]. Our group and others later demonstrated that loss of murine Panx1 channels causes
625 enhanced and functional modifications of synapses encompassing increased hippocampal
626 excitability, complex dendritic branching, enhanced spine maturation, and an increased proportion
627 of multiple synaptic contacts in hippocampal neurons of Panx1-KO mice [42,63,64]. Moreover, under
628 genetic conditions associated with NDDs, suppression of Panx1 can restore synaptic plasticity.
629 Specifically, in a transgenic Alzheimer's Disease model, pharmacological blocking of Panx1
630 significantly reduced excitatory synaptic defects by normalizing long-term potentiation (LTP) and
631 depression (LTD) and improving dendritic arborization and spine density in hippocampal neurons
632 [65]. Genetic ablation of Panx1 suggested that Panx1 negatively regulated cortical dendritic spines
633 development [16]. In the visual system, Panx1 channels contribute to synaptic modulation of a
634 horizontal cell to photoreceptor feedback mechanism in horizontal cell dendrites of the mouse and
635 the zebrafish [66,67,68]. Furthermore, loss of Panx1 caused altered learning and memory in mice such
636 as diminished cognitive functions including altered spatial reference memory, or spatial reversal
637 learning [42,63,69,41]. Collectively, these studies demonstrate a regulatory role for Panx1 in modulating
638 synapse development, refinement, and plasticity such that reduction of Panx1 generally enhances
639 synapse properties while maintaining neural circuit balance required for cognitive function within
640 the CNS.

641 Despite accumulating evidence for roles of Panx1 in synaptic plasticity, mechanistic details
642 of the cellular processes and molecular pathways is emerging slowly. Internalization of Panx1 by
643 ATP and P2X7-dependent endocytosis and degradation [70,71] and suppression of presynaptic
644 glutamate release via NMDA receptors and Panx1 have been reported [72]. Panx1 coupling to NMDA
645 receptor functions via Src [28], STIM1/2 [26] or actin, and Rho GTPases, appear to be relevant for

646 synapse stability [64]. Panx1 channel blockage with the mimetic peptide [10]Panx1 increases the
647 synaptic level of endocannabinoids (eCB) and the activation of cannabinoid receptors type 1
648 (CB1Rs), decreasing hippocampal GABAergic efficacy and shifting excitation/inhibition (E/I)
649 balance toward excitation and facilitating the induction of long-term potentiation [73]. Further, we
650 have reported a pathway that connects NMDA receptor signaling to the opening of electrical
651 synapse protein Cx36 via Panx1 and CaMK2a, suggesting active participation of Panx1 in
652 modulating both chemical and electrical synapse function by using a shared molecular machinery
653 [74].

654 In summary, our novel results highlight the significance of Panx1 channels in synaptic
655 transmission and organization, particularly in metabolically challenged zebrafish. The results
656 further underscore Panx1's involvement in transsynaptic activities. The observable molecular,
657 behavioral, and electrophysiological deficits, provide insights into the functional consequences of
658 Panx1 modulation at synaptic and neural circuit levels. The results from zebrafish and mouse
659 models allows for cross-species comparisons, and they suggest an evolutionary conservation of
660 Panx1 function and its diverse roles in synaptic physiology.

661

662 ***Panx1a integrates cellular homeostasis with mitochondrial health.***

663 MPTP (1-methyl-4-phenyl-1,2,3,6-tetrahydropyridine) treatment has been extensively studied
664 within the context of molecular pathways leading to neurodegenerative disorders. MPTP inhibits
665 Complex I of the mitochondrial electron transport chain. Evidence that mitochondrial
666 perturbation is a driver of synaptic dysfunction has been previously reported for AD [75], PD [76,77],
667 ALS [78,79], and HD [80,81]. Our main results recapitulate the common deficits following MPTP
668 treatment such as activation of reactive oxygen species pathways, impaired oxidative

669 phosphorylation, ATP loss, defective mitochondrial homeostasis, or the unfolded protein
670 response.

671 Direct functions of Panx1 in cellular homeostasis and mitochondrial health in the nervous
672 system *in vivo* have not been formally established, and there is not yet a complete mechanistic
673 explanation for how Panx1 channels function as a molecular platform for converging signaling
674 pathways. We would like to propose that Panx1a acts as a sensor, akin to a "rheostat" opening
675 and closing depending on the metabolic state. By functioning as a molecular regulator with
676 graded effects, Panx1 can modulate cellular responses in a context-dependent manner. It is
677 tempting to speculate that the known structural aspects, such as functioning as a large pore ATP
678 release channel, or a narrow Cl channel [82,83], or interacting with different lipid environments [84], or
679 interacting proteins [46], contribute to observed alterations.

680

681 ***Loss of Panx1 intensifies the execution phase of cell death.***

682 We recently described low extracellular ATP concentrations in the Panx1a$^{-/-}$ fish in an
683 experimental model of epilepsy [39]. Whereas genetic ablation and pharmacological blocking of
684 Panx1 reduced the seizure risk in 6dpf larvae with no evidence for cell death, similarly low levels
685 of ATP after MPTP treatment in our new study triggered pathways, most prominently those
686 converging on the mammalian target of rapamycin (mTORC1) complex, leading to cell death.
687 The different consequences seen in the two experimental models is of significance considering
688 that the identical fish line was used.

689 mTOR controls many basic cellular functions such as protein synthesis, energy
690 metabolism, cell size, lipid metabolism, autophagy, mitochondria, and lysosome biogenesis. In
691 addition, mTOR-controlled signaling pathways regulate many integrated physiological functions
692 of the nervous system including neuronal development, synaptic plasticity, memory storage, and

693 cognition [85]. The perturbation of the mTOR signaling cascade is a common pathophysiological
694 feature of neurological and neuropsychiatric disorders [86]. Here, the demonstrated alterations to
695 the composition of synapses, energy homeostasis, and pathways regulating cell death including
696 autophagy and apoptosis align with the roles of mTOR signaling.

697 They also align with mTOR functions in Mammalia influenced by the activities of
698 neuronal surface receptors and channels including N-methyl-D-aspartate receptors (NMDA
699 receptors), α-amino-3-hydroxy-5-methyl-4-isoxazolepropionic acid receptors (AMPA receptors),
700 brain-derived neurotropic factor (BDNF), and dopaminergic and metabotropic glutamate
701 receptors (mGluRs), which are vital for biophysical properties of neuronal networks like the
702 induction and maintenance of LTP and LTD. Together, the reduced expression of NMDA
703 receptors, AMPA receptors, changes to biophysical properties, and the increase in cell death align
704 with work in higher vertebrates.

705 mTOR also acts as a node of convergence downstream of these receptors and several
706 signaling pathways that include phosphoinositide-dependent kinase-1 (PDK1),
707 phosphatidylinositol 3-kinase (PI3K) [87], Akt [88], and tuberous sclerosis complex proteins 1 and 2
708 (Tsc1/2) [89,90]. We excluded the differential expression regulation of these pathways since they did
709 not meet our threshold criteria. Furthermore, late endosomal/lysosomal adaptor and MAPK and
710 mTOR activator genes (LAMTOR/Ragulator) were found that can regulate multiprotein signaling
711 units on late endosomes/lysosomes involved in acidification (*lamtor2, lamtor3, lamtor5*). In
712 short, the transcriptional profiling in this study identified a profound dysregulation of these
713 downstream pathways and genes. At the interface of metabolic pathways, the autophagy-
714 lysosomal pathway functions to respond to reactive oxygen species that are generated from
715 perturbations of cellular glucose metabolism and bioenergetic function. They maintain
716 mitochondrial quality and generally serve an important protective function.

717 Our research also provides insight into the interplay between Panx1a, cellular signaling,
718 energy metabolism, and calcium homeostasis in safeguarding neuronal health. We provide
719 evidence that the absence of Panx1 exacerbates cellular death by intensifying repercussions of
720 low intracellular ATP levels. The depletion of ATP induces apoptosis, a programmed form of cell
721 death, by impairing the function of ATP-dependent enzymes like caspases, thereby disrupting the
722 delicate balance between pro-apoptotic and anti-apoptotic proteins.

723 Notably, Panx1a depletion disturbs the delicate equilibrium between excitatory and
724 inhibitory signals, exacerbating neuronal dysfunction and ultimately leading to increased rates of
725 cell death.

726 Low ATP levels play a pivotal role in triggering cell death pathways through various
727 mechanisms. One such pathway involves the activation of the AMP-activated Protein Kinase
728 (AMPK), an energy sensor within cells. While AMPK activation initially aims to restore ATP
729 levels by inhibiting anabolic processes and stimulating catabolic pathways, prolonged activation
730 can induce cell death via pro-apoptotic protein activation. Additionally, ATP depletion can lead
731 to Endoplasmic Reticulum (ER) stress, initiating the unfolded protein response (UPR). While the
732 UPR aims to restore protein homeostasis, persistent or severe ER stress can trigger apoptotic
733 pathways.

734 Specifically, Panx1 channels modulate calcium signaling and are subject to regulation by
735 calcium-activated kinases such as SRC and CaMKII. The proposed rheostat model suggests that
736 Panx1 can control calcium influx into cells in a feedback loop with NMDA receptors, thereby
737 maintaining calcium homeostasis and preventing excessive calcium entry-induced neurotoxicity.

738 In summary, the main findings emphasize the critical importance of Panx1 in preserving
739 neuronal viability by regulating energy metabolism, facilitating cellular communication, and
740 maintaining calcium homeostasis. Understanding the intricate interplay between Panx1 and

741 cellular pathways implicated in neurodegeneration could provide crucial insights for the
742 development of targeted interventions against neurodegenerative diseases.
743

744 **Conclusion**

745 The pathways to neurodegenerative disorders are inherently complex with pathological changes
746 often not noticed until later in live with the onset of clinical symptoms. Our study presents a
747 single snapshot on Panx1a function early in life when a whole organism is treated with MPTP.
748 The wealth of computational and experimental data opens a window of opportunity to investigate
749 the roles of Panx1a across the lifespan. A longitudinal study from larvae to adult fish using the
750 acute MPTP zebrafish model is feasible. Other practical and immediately executable tests will
751 use pharmacological interference with the mTORC1 pathway, autophagy, or Wnt/ß-catenin
752 signaling to investigate how dampening the cellular, bioelectrical, and behavioral alterations to
753 energy and cellular homeostasis affect the observed phenotype in the absence of Panx1a. This
754 suggests that consistent with other approaches for treating NDDs, namely NMDA receptor
755 modulation, a tenable strategy would be through modulation of Panx1 function, for example by
756 fine-tuning of Panx1 expression and disorder-specifc signaling pathways. In conclusion, the
757 primary findings shed light on the multifaceted role of Panx1a in orchestrating cellular
758 homeostasis and mitigating neurodegenerative pathways. By elucidating its contributions to
759 diverse neurodegenerative disorders, we unveil Panx1a as a potential therapeutic target for
760 interventions aimed at modulating neuronal health and combating neurodegeneration.
761

762 **Materials and Methods**

763 **Zebrafish lines.** Zebrafish (*Danio Rerio*) of strain Tubingen long fin (TL) were maintained in
764 groups with mixed sex in a recirculation system (Aquaneering Inc., San Diego, CA) at 28ºC on a
765 14hr light/10hr dark cycle. All animal work was performed at York University's zebrafish

766 vivarium and in an S2 biosafety laboratory following the Canadian Council for Animal Care
767 guidelines after approval of the study protocol by the York University Animal Care Committee
768 (GZ#2019-7-R2). The *Panx1a* knockout line (*panx1a*$^{-/-}$) was generated and characterized in-
769 house [44,91,92].
770
771 **Zebrafish Locomotion Assays**. The Zebrabox behavior system and the ZebraLab analytical suite
772 (ViewPoint Life Technology, Lyon, France, http://www.viewpoint.fr) were used for automated
773 extraction of behavioral outputs and video tracking. Tracking videos were recorded at 30 frames
774 per second (fps) under infrared (for Light-OFF recording) or visible light (Light-ON)
775 illumination using a Point Grey Research Dragonfly2 DR2-HIBW camera (Teledyne-FLIR,
776 Burlington, ON, Canada). Inside the Zebrabox a lightbox provided visible and infrared light from
777 below for recordings up to 40% light intensity (visible range, 0-1200 lux). 6dpf larvae were
778 observed in clear 48-well plates maintained at 28ºC throughout the experiment. All experiments
779 were performed between 12:00 to 2 pm, as larvae (6 dpf) activity was previously reported to
780 reach a stable level by early afternoon [93]. Locomotor activity scores (total distance ± SEM.; n =
781 16 per group) were determined from larvae's movements in the time window from 2100 to 2300
782 seconds. Panx1a$^{+/+}$ and Panx1a$^{-/-}$ larvae were exposed to MPTP (Sigma-Aldrich) for four hours
783 prior to recording. The Zebrabox provided a Light-OFF stimulus for 20 minutes at 0% intensity
784 (0 lux), followed by incremental 10% light intensity increases every 10 minutes up to 40% (1200
785 lux). A principal component analysis (PCA) was performed as described [44,94]. The statistical
786 analysis of locomotion data used a Welch's t-test.
787
788 ***In vivo* electrophysiology.** Published procedures were used to prepare anaesthetized 6 days post
789 fertilization (6dpf) zebrafish larvae for *in vivo* electrophysiology [44,95]. Zebrafish larvae at 6dpf
790 were anesthetized using 0.3mM Pancuronium bromide (Sigma-Aldrich, Oakville, ON, Canada)
791 for 2-3 min until the touch response stopped. Anesthetized larvae were immobilized in freshly
792 prepared 2% low melting temperature agarose. A Leica S9E dissecting microscope (Leica
793 Microsystems, Richmond Hill, ON, Canada) was used to orient the dorsal aspect of the larvae to
794 the gel surface. Embedded larvae were placed on the upright stage of an Olympus BX51
795 fluorescence microscope (Olympus, Richmond Hill, ON, Canada). Larvae were submerged in
796 1ml of egg water (E3; pH 7.2-7.4) that was applied topically to the agar. Under direct visual
797 guidance two glass microelectrodes (1.2mM OD, approximately 1µM tip diameter, 2-7MΩ),

backloaded with 2M NaCl, were placed into the right optic tectum (OT) and the dorsomedial (DM) region of the pallium. Local field potentials were recorded simultaneously from both microelectrodes using a Multiclamp 700B amplifier (Axon Instruments, San Jose, CA, USA). Voltage recordings were low-pass filtered at 1kHz (-3 dB; eight-pole Bessel), high-pass filtered at 0.1 Hz, digitized at 10 kHz using a Digidata 1550A A/D interface, and stored on a PC running pClamp11 software (all Axon Instruments). The basal activity was recorded for 10 minutes under Light-ON conditions (1000 lux), during which images of the electrode placement were taken for reference. For each fish, brain activity was normalized to its baseline activity to account for the biological variability of individual brains. In the treatment group larvae were exposed to MPTP (50µM) four hours before recording. A temperature of 28ºC was maintained during experiments.

Power spectral density and coherence detection analysis. A Power spectral density (PSD) estimation was performed by the Welch's method for baseline and MPTP recordings. A moving window for fast Fourier transform (FFT) computation was used and all windows were averaged. The frequency bands theta (3.5-7.5 Hz), beta (12-30 Hz) and gamma (35-45 Hz) were extracted for analysis using NeuroExplorer Version 4 (Nex Technologies, Colorado Springs, CO, 80906, USA). Changes in PSD between baseline and treatment were analyzed for significance using a Welch's t-test. A Coherence analysis was performed applying the Hann method for baseline and MPTP recordings using NeuroExplorer. Changes in the coherence between baseline and treatment were tested for significance using a Welch's t-test.

Extracellular ATP Assay. For quantification of ATP and protein ≈ 50 6dpf larvae were collected at experimental endpoints. Larvae were homogenized in 500µl ice-cold of Phosphate-Buffered Saline (PROBS) containing 100µM ARL-67156 (Sigma-Aldrich) and Halt Protease inhibitor (1:100) (Thermo-Fisher Scientific, Waltham, Massachusetts, USA) for 1min at 30Hz using the Tissuelyser^{LT} (Qiagen, Hilden, Germany). Homogenates were transferred to chilled Eppendorf tubes ($^{-}$20ºC) and centrifuged at 12,000 rpm for 2min. Supernatants were collected and snap-frozen in liquid nitrogen before storage at $^{-}$80ºC. Extracellular ATP measurements used a 96-well format (Greiner Bio-One, Monroe, North Carolina, USA) and the Molecular PROBes® ATP determination Kit as described by the manufacturer (Life Technologies, Burlington, ON, Canada). ATP was quantified in replicates of 6 using the Synergy H4 Hybrid Multi-well Plate Reader (Biotek, Winooski, Vermont, USA). The luminescent assay parameters were: plate

830 temperature set to 28ºC; a low-intensity shake of the plate for 3s before reading; a 5s integration
831 time per well; gain setting at 150. In every test, the ATP concentration in experimental samples
832 was calculated from ATP standard curves (0-1µM ATP) included in the same 96-well plate. Data
833 were exported from the Gen5 Data Analysis Software (Biotek) and analyzed in Excel and
834 GraphPad Prism 10. ATP was represented as a normalized concentration per mg of protein. A
835 NanoDrop Spectrophotometer (Thermo Fisher Scientific) was used to measure protein content in
836 2µL of supernatant from homogenized samples. The final ATP content was expressed after
837 normalizing the protein content in each sample of pooled larvae [11]. The data sets were compared
838 using a Welch's t-test.
839
840 **Cell Death Assay.** Up to seven larvae (6dpf) were placed into a 2ml Eppendorf tube in egg
841 water. MPTP treatment (20µM) was applied for four hours. During the last 60mins, acridine
842 orange (2.5µl/ml; Sigma-Aldrich) was added to the Eppendorf tube. Following incubation, the
843 larvae freely swam in 10ml fresh egg water for 10 minutes to remove excess AO. Then, the
844 larvae were immobilized using the muscle relaxant pancuronium bromide and mounted head
845 down in 2% agar noble in dishes. Cell death was imaged using a Zeiss LSM700 (Objective 10x
846 NA0.8; Z-stack ≈ 100µm). All parameters were controlled by ZEN software (ZEISS, North York,
847 ON, Canada) and consistently applied. Raw 3D volumes were processed for AO-positive cell
848 detection using Bitplane-Imaris software (Oxford Instruments, Abingdon, UK). Statistics used
849 unpaired t-test and GraphPad Prism 10.
850
851 **NGS RNA-sequencing.** The transcriptomes of all zebrafish lines used in this research were
852 analyzed by RNA-seq (NGS-Facility, The Center for Applied Genomics, SickKids, Toronto, ON,
853 Canada). The reported data was derived from the sequencing of three independent pools of ≈30
854 age-matched larvae (6dpf). The RNA-seq data are deposited at the NCBI - Gene Expression
855 Omnibus (GEO) database repository (ID pending). Total RNAs were extracted from 30 6dpf
856 larvae using RNeasy Plus Mini Kit (Qiagen). The RNA quality was determined using a
857 Bioanalyzer 2100 DNA High Sensitivity chip (Agilent Technologies, Mississauga, ON, Canada).
858 The RNA library preparation was performed following the NEB NEBNext Ultra II Directional
859 RNA Library Preparation protocol (New England Biolabs Inc., Ipswich, MA, USA). RNA
860 libraries were loaded on a Bioanalyzer 2100 DNA High Sensitivity chip to check for size,
861 quantified by qPCR using the Kapa Library Quantification Illumina/ABI Prism Kit protocol

862 (KAPA Biosystems, Wilmington, MA, USA). Pooled libraries were paired-end sequenced on a
863 High Throughput Run Mode flow cell with the V4 sequencing chemistry on an Illumina HiSeq
864 2500 platform (Illumina, Inc., San Diego, CA) following Illumina's recommended protocol to
865 generate paired-end reads of 126-bases in length.
866
867 **Differential Gene Expression and Functional Enrichment Analyses.** The post-sequencing
868 processing to final read counts, normalization, and differential gene expression analysis used
869 multiple software packages, including a two-condition differential expression analysis using the
870 edgeR R-package, v.3.8.6 () [96,97] and DESeq2 R package version 1.40.2 [98]. Genotypes and
871 treatments were incorporated into the statistical model and multiple hypothesis testing was
872 performed. The default filter for DESeq2 used a threshold of $p<0.05$ and the Benjamini-Hochberg
873 procedure to determine the false discovery rate (FDR), and the adjusted P-value (padj).
874 Differential gene expression was defined as log2FoldChange >2 or <-2, respectively.
875 A Gene Set Variation Analysis (GSEA) tested whether a defined set of genes shows
876 statistically significant, concordant differences between genotypes and treatment groups. This
877 method calculates sample-wise gene set enrichment scores and estimates variation of pathway
878 activity over a sample population in an unsupervised manner [98]. The Molecular Signatures
879 Database (MSigDB) v.5.2 (http://software.broadinstitute.org/gsea/msigdb/index.jsp), a renowned
880 repository of curated gene sets encompassing diverse biological pathways was used to source
881 gene sets for broad Hallmarks. Before GSEA RNAseq data were filtered at padj < 0.01 to
882 increase the stringency of the analysis. Other tools used to process RNAseq data were HCOP
883 (https://www.genenames.org/tools/hcop/) and db2db at bioDBnet
884 (https://biodbnet.abcc.ncifcrf.gov/db/db2db.php) to convert curated human or mouse to zebrafish
885 genes [99,100]. Curated gene lists were generate with information from the Zebrafish Information
886 Network (ZFIN) (https://zfin.org/) and the KEGG (Kyoto Encyclopedia of Genes and Genomes,
887 https://www.genome.jp/kegg/) databases, and using unique qualifiers from the Gene Ontology
888 (GO) project (https://geneontology.org/).
889
890 **Pharmacology**. All chemicals were purchased from Sigma-Aldrich (Mississauga, Canada):
891 (MPTP; 1-50µM; cat#: M0896), Pancuronium bromide (Panc; 300µM; cat#P1918), Acridine-
892 Orange (AO; 15µM; cat#: A6014). All reagents were water-soluble. All concentrations referred
893 to in the results section are final.

894

895 **Statistics and data reproducibility.** All statistical analyses were performed in NeuroExplorer
896 VS4, or in GraphPad Prism VS10. Results are represented as the mean ± standard error of the
897 mean (SEM). For each analysis, a minimum of $n \geq 3$ independent experimental replicates were
898 generated. The normality and homogeneity of the data variance were determined by the "Shapiro-
899 Wilk Test" and "Levene's Test." A P value <0.05 was considered statistically significant. For all
900 experiments, sample sizes, statistical tests, and when appropriate P values are indicated in the
901 figure legends.
902

903 **Acknowledgements.** We thank two members of York University Zebrafish Vivarium, Janet
904 Fleites-Medina, and Veronica Scavo for outstanding zebrafish husbandry. We also wish to thank
905 the team at the Center for Applied Genomics, SickKids, Toronto, ON, Canada for assistance with
906 RNA-seq. This research was supported by the Natural Sciences and Engineering Research
907 Council (NSERC) discovery grant RGPIN-2019-06378 (GRZ).
908

909 **Author contributions.** Conceptualization, GSZ, GRZ; data analysis, GSZ, NS, GRZ;
910 investigation, GSZ, NS, CZ; writing—original draft preparation, GSZ, GRZ; writing—review
911 and editing, all authors; visualization, GSZ, NS, GRZ; supervision, SC, GRZ; project
912 administration, GRZ; funding acquisition, GRZ. All authors have read and agreed to the
913 published version of the manuscript.
914

915 **Data Availability.** The RNA-seq data are deposited at the NCBI - Gene Expression Omnibus
916 (GEO) database repository (ID pending).
917

918 **Competing interests.** The authors declare no competing interests.
919

920 **Materials & Correspondence.** Correspondence and material requests should be addressed to
921 Georg R. Zoidl.
922
923
924
925

References

1 Wilson, D. M., 3rd *et al.* Hallmarks of neurodegenerative diseases. *Cell* **186**, 693-714 (2023). https://doi.org/10.1016/j.cell.2022.12.032

2 Jack, C. R., Jr. *et al.* NIA-AA Research Framework: Toward a biological definition of Alzheimer's disease. *Alzheimers Dement* **14**, 535-562 (2018). https://doi.org/10.1016/j.jalz.2018.02.018

3 Mattson, M. P., Pedersen, W. A., Duan, W., Culmsee, C. & Camandola, S. Cellular and molecular mechanisms underlying perturbed energy metabolism and neuronal degeneration in Alzheimer's and Parkinson's diseases. *Ann N Y Acad Sci* **893**, 154-175 (1999). https://doi.org/10.1111/j.1749-6632.1999.tb07824.x

4 Spinelli, J. B. & Haigis, M. C. The multifaceted contributions of mitochondria to cellular metabolism. *Nat Cell Biol* **20**, 745-754 (2018). https://doi.org/10.1038/s41556-018-0124-1

5 Golpich, M. *et al.* Mitochondrial Dysfunction and Biogenesis in Neurodegenerative diseases: Pathogenesis and Treatment. *CNS Neurosci Ther* **23**, 5-22 (2017). https://doi.org/10.1111/cns.12655

6 Jadiya, P., Garbincius, J. F. & Elrod, J. W. Reappraisal of metabolic dysfunction in neurodegeneration: Focus on mitochondrial function and calcium signaling. *Acta Neuropathol Commun* **9**, 124 (2021). https://doi.org/10.1186/s40478-021-01224-4

7 Boassa, D. *et al.* Pannexin1 channels contain a glycosylation site that targets the hexamer to the plasma membrane. *J Biol Chem* **282**, 31733-31743 (2007). https://doi.org/10.1074/jbc.M702422200

8 Penuela, S. *et al.* Pannexin 1 and pannexin 3 are glycoproteins that exhibit many distinct characteristics from the connexin family of gap junction proteins. *J Cell Sci* **120**, 3772-3783 (2007). https://doi.org/10.1242/jcs.009514

9 Penuela, S., Bhalla, R., Nag, K. & Laird, D. W. Glycosylation regulates pannexin intermixing and cellular localization. *Mol Biol Cell* **20**, 4313-4323 (2009). https://doi.org/10.1091/mbc.e09-01-0067

10 Bruzzone, R., Hormuzdi, S. G., Barbe, M. T., Herb, A. & Monyer, H. Pannexins, a family of gap junction proteins expressed in brain. *Proc Natl Acad Sci U S A* **100**, 13644-13649 (2003). https://doi.org/10.1073/pnas.2233464100

11 Whyte-Fagundes, P. *et al.* A Potential Compensatory Role of Panx3 in the VNO of a Panx1 Knock Out Mouse Model. *Front Mol Neurosci* **11**, 135 (2018). https://doi.org/10.3389/fnmol.2018.00135

12 Ruan, Z., Orozco, I. J., Du, J. & Lu, W. Structures of human pannexin 1 reveal ion pathways and mechanism of gating. *Nature* **584**, 646-651 (2020). https://doi.org/10.1038/s41586-020-2357-y

13 Michalski, K. *et al.* The Cryo-EM structure of pannexin 1 reveals unique motifs for ion selection and inhibition. *Elife* **9** (2020). https://doi.org/10.7554/eLife.54670

14 Sanchez-Arias, J. C., Candlish, R. C., van der Slagt, E. & Swayne, L. A. Pannexin 1 Regulates Dendritic Protrusion Dynamics in Immature Cortical Neurons. *eNeuro* **7** (2020). https://doi.org/10.1523/ENEURO.0079-20.2020

15 Wicki-Stordeur, L. E., Dzugalo, A. D., Swansburg, R. M., Suits, J. M. & Swayne, L. A. Pannexin 1 regulates postnatal neural stem and progenitor cell proliferation. *Neural Dev* **7**, 11 (2012). https://doi.org/10.1186/1749-8104-7-11

16 Sanchez-Arias, J. C. *et al.* Pannexin 1 Regulates Network Ensembles and Dendritic Spine Development in Cortical Neurons. *eNeuro* **6** (2019). https://doi.org/10.1523/ENEURO.0503-18.2019

17 Weickert, S., Ray, A., Zoidl, G. & Dermietzel, R. Expression of neural connexins and pannexin1 in the hippocampus and inferior olive: a quantitative approach. *Brain Res Mol Brain Res* **133**, 102-109 (2005). https://doi.org/10.1016/j.molbrainres.2004.09.026

18 Ray, A., Zoidl, G., Wahle, P. & Dermietzel, R. Pannexin expression in the cerebellum. *Cerebellum* **5**, 189-192 (2006). https://doi.org/10.1080/14734220500530082

19 Ray, A., Zoidl, G., Weickert, S., Wahle, P. & Dermietzel, R. Site-specific and developmental expression of pannexin1 in the mouse nervous system. *Eur J Neurosci* **21**, 3277-3290 (2005). https://doi.org/10.1111/j.1460-9568.2005.04139.x

20 Ding, Z. *et al.* Emerging Roles of Microglia in Neuro-vascular Unit: Implications of Microglia-Neurons Interactions. *Front Cell Neurosci* **15**, 706025 (2021). https://doi.org/10.3389/fncel.2021.706025

21 Pelegrin, P., Barroso-Gutierrez, C. & Surprenant, A. P2X7 receptor differentially couples to distinct release pathways for IL-1beta in mouse macrophage. *J Immunol* **180**, 7147-7157 (2008). https://doi.org/10.4049/jimmunol.180.11.7147

22 Chekeni, F. B. *et al.* Pannexin 1 channels mediate 'find-me' signal release and membrane permeability during apoptosis. *Nature* **467**, 863-867 (2010). https://doi.org/10.1038/nature09413

23 Silverman, W. R. *et al.* The pannexin 1 channel activates the inflammasome in neurons and astrocytes. *J Biol Chem* **284**, 18143-18151 (2009). https://doi.org/10.1074/jbc.M109.004804

24 Poon, I. K. *et al.* Unexpected link between an antibiotic, pannexin channels and apoptosis. *Nature* **507**, 329-334 (2014). https://doi.org/10.1038/nature13147

25 Sandilos, J. K. *et al.* Pannexin 1, an ATP release channel, is activated by caspase cleavage of its pore-associated C-terminal autoinhibitory region. *J Biol Chem* **287**, 11303-11311 (2012). https://doi.org/10.1074/jbc.M111.323378

26 Patil, C. S. *et al.* ER-resident STIM1/2 couples Ca(2+) entry by NMDA receptors to pannexin-1 activation. *Proc Natl Acad Sci U S A* **119**, e2112870119 (2022). https://doi.org/10.1073/pnas.2112870119

27 Lopez, X. *et al.* A physiologic rise in cytoplasmic calcium ion signal increases pannexin1 channel activity via a C-terminus phosphorylation by CaMKII. *Proc Natl Acad Sci U S A* **118** (2021). https://doi.org/10.1073/pnas.2108967118

28 Weilinger, N. L. *et al.* Metabotropic NMDA receptor signaling couples Src family kinases to pannexin-1 during excitotoxicity. *Nat Neurosci* **19**, 432-442 (2016). https://doi.org/10.1038/nn.4236

29 Thompson, R. J., Zhou, N. & MacVicar, B. A. Ischemia opens neuronal gap junction hemichannels. *Science* **312**, 924-927 (2006). https://doi.org/10.1126/science.1126241

1012 30 MacVicar, B. A. & Thompson, R. J. Non-junction functions of pannexin-1 channels. *Trends*
1013 *Neurosci* **33**, 93-102 (2010). https://doi.org/10.1016/j.tins.2009.11.007
1014 31 Thompson, R. J. *et al.* Activation of pannexin-1 hemichannels augments aberrant
1015 bursting in the hippocampus. *Science* **322**, 1555-1559 (2008).
1016 https://doi.org/10.1126/science.1165209
1017 32 Chen, P. Y. *et al.* Neuronal NLRP3 inflammasome mediates spreading depolarization-
1018 evoked trigeminovascular activation. *Brain* **146**, 2989-3002 (2023).
1019 https://doi.org/10.1093/brain/awad045
1020 33 Chen, S. P. *et al.* Inhibition of the P2X7-PANX1 complex suppresses spreading
1021 depolarization and neuroinflammation. *Brain* **140**, 1643-1656 (2017).
1022 https://doi.org/10.1093/brain/awx085
1023 34 Vasile, F. *et al.* Pannexin 1 activity in astroglia sets hippocampal neuronal network
1024 patterns. *PLoS Biol* **20**, e3001891 (2022). https://doi.org/10.1371/journal.pbio.3001891
1025 35 Weilinger, N. L. *et al.* Pannexin-1 opening in neuronal edema causes cell death but also
1026 leads to protection via increased microglia contacts. *Cell Rep* **42**, 113128 (2023).
1027 https://doi.org/10.1016/j.celrep.2023.113128
1028 36 Xu, X. *et al.* Probenecid Disrupts a Novel Pannexin 1-Collapsin Response Mediator
1029 Protein 2 Interaction and Increases Microtubule Stability. *Front Cell Neurosci* **12**, 124
1030 (2018). https://doi.org/10.3389/fncel.2018.00124
1031 37 Wicki-Stordeur, L. E. & Swayne, L. A. Panx1 regulates neural stem and progenitor cell
1032 behaviours associated with cytoskeletal dynamics and interacts with multiple
1033 cytoskeletal elements. *Cell Commun Signal* **11**, 62 (2013). https://doi.org/10.1186/1478-
1034 811X-11-62
1035 38 Aquilino, M. S. *et al.* Pannexin-1 Deficiency Decreases Epileptic Activity in Mice. *Int J Mol*
1036 *Sci* **21** (2020). https://doi.org/10.3390/ijms21207510
1037 39 Whyte-Fagundes, P. *et al.* Panx1 channels promote both anti- and pro-seizure-like
1038 activities in the zebrafish via p2rx7 receptors and ATP signaling. *Commun Biol* **5**, 472
1039 (2022). https://doi.org/10.1038/s42003-022-03356-2
1040 40 Obot, P., Velisek, L., Veliskova, J. & Scemes, E. The Contribution of Astrocyte and
1041 Neuronal Panx1 to Seizures Is Model and Brain Region Dependent. *ASN Neuro* **13**,
1042 17590914211007273 (2021). https://doi.org/10.1177/17590914211007273
1043 41 Obot, P. *et al.* Astrocyte and Neuronal Panx1 Support Long-Term Reference Memory in
1044 Mice. *ASN Neuro* **15**, 17590914231184712 (2023).
1045 https://doi.org/10.1177/17590914231184712
1046 42 Prochnow, N. *et al.* Pannexin1 stabilizes synaptic plasticity and is needed for learning.
1047 *PLoS One* **7**, e51767 (2012). https://doi.org/10.1371/journal.pone.0051767
1048 43 Dong, H. *et al.* Transient MPTP exposure at a sensitive developmental window altered
1049 gut microbiome and led to male-biased motor and social behavioral deficits in adult
1050 zebrafish. *Neurotoxicology* **91**, 360-368 (2022).
1051 https://doi.org/10.1016/j.neuro.2022.06.008
1052 44 Safarian, N., Whyte-Fagundes, P., Zoidl, C., Grigull, J. & Zoidl, G. Visuomotor deficiency in
1053 panx1a knockout zebrafish is linked to dopaminergic signaling. *Sci Rep* **10**, 9538 (2020).
1054 https://doi.org/10.1038/s41598-020-66378-y

45 Subramanian, A. *et al.* Gene set enrichment analysis: a knowledge-based approach for interpreting genome-wide expression profiles. *Proc Natl Acad Sci U S A* **102**, 15545-15550 (2005). https://doi.org/10.1073/pnas.0506580102

46 Frederiksen, S. D., Wicki-Stordeur, L. E. & Swayne, L. A. Overlap in synaptic neurological condition susceptibility pathways and the neural pannexin 1 interactome revealed by bioinformatics analyses. *Channels (Austin)* **17**, 2253102 (2023). https://doi.org/10.1080/19336950.2023.2253102

47 Bloch, S. *et al.* Non-thalamic origin of zebrafish sensory nuclei implies convergent evolution of visual pathways in amniotes and teleosts. *Elife* **9** (2020). https://doi.org/10.7554/eLife.54945

48 Mueller, T. What is the Thalamus in Zebrafish? *Front Neurosci* **6**, 64 (2012). https://doi.org/10.3389/fnins.2012.00064

49 Asadi, A., Madadi Asl, M., Vahabie, A. H. & Valizadeh, A. The Origin of Abnormal Beta Oscillations in the Parkinsonian Corticobasal Ganglia Circuits. *Parkinsons Dis* **2022**, 7524066 (2022). https://doi.org/10.1155/2022/7524066

50 Nurislamova, Y. M., Novikov, N. A., Zhozhikashvili, N. A. & Chernyshev, B. V. Enhanced Theta-Band Coherence Between Midfrontal and Posterior Parietal Areas Reflects Post-feedback Adjustments in the State of Outcome Uncertainty. *Front Integr Neurosci* **13**, 14 (2019). https://doi.org/10.3389/fnint.2019.00014

51 Toni, M. & Cioni, C. Fish Synucleins: An Update. *Mar Drugs* **13**, 6665-6686 (2015). https://doi.org/10.3390/md13116665

52 Sun, Z. & Gitler, A. D. Discovery and characterization of three novel synuclein genes in zebrafish. *Dev Dyn* **237**, 2490-2495 (2008). https://doi.org/10.1002/dvdy.21569

53 Milanese, C. *et al.* Hypokinesia and reduced dopamine levels in zebrafish lacking beta- and gamma1-synucleins. *J Biol Chem* **287**, 2971-2983 (2012). https://doi.org/10.1074/jbc.M111.308312

54 Beyer, K. *et al.* The decrease of beta-synuclein in cortical brain areas defines a molecular subgroup of dementia with Lewy bodies. *Brain* **133**, 3724-3733 (2010). https://doi.org/10.1093/brain/awq275

55 Zhang, C. C., Xing, A., Tan, M. S., Tan, L. & Yu, J. T. The Role of MAPT in Neurodegenerative Diseases: Genetics, Mechanisms and Therapy. *Mol Neurobiol* **53**, 4893-4904 (2016). https://doi.org/10.1007/s12035-015-9415-8

56 Dubey, J., Ratnakaran, N. & Koushika, S. P. Neurodegeneration and microtubule dynamics: death by a thousand cuts. *Front Cell Neurosci* **9**, 343 (2015). https://doi.org/10.3389/fncel.2015.00343

57 Caillet-Boudin, M. L., Buee, L., Sergeant, N. & Lefebvre, B. Regulation of human MAPT gene expression. *Mol Neurodegener* **10**, 28 (2015). https://doi.org/10.1186/s13024-015-0025-8

58 Lau, P. *et al.* Alteration of the microRNA network during the progression of Alzheimer's disease. *EMBO Mol Med* **5**, 1613-1634 (2013). https://doi.org/10.1002/emmm.201201974

59 Moussavi Nik, S. H. *et al.* Hypoxia alters expression of zebrafish microtubule-associated protein tau (mapta, maptb) gene transcripts. *BMC Res Notes* **7**, 767 (2014). https://doi.org/10.1186/1756-0500-7-767

1099 60 Jia, L., Pina-Crespo, J. & Li, Y. Restoring Wnt/beta-catenin signaling is a promising
1100 therapeutic strategy for Alzheimer's disease. *Mol Brain* **12**, 104 (2019).
1101 https://doi.org/10.1186/s13041-019-0525-5
1102 61 Sayedyahossein, S. *et al.* Pannexin 1 binds beta-catenin to modulate melanoma cell
1103 growth and metabolism. *J Biol Chem* **296**, 100478 (2021).
1104 https://doi.org/10.1016/j.jbc.2021.100478
1105 62 Zoidl, G. *et al.* Localization of the pannexin1 protein at postsynaptic sites in the cerebral
1106 cortex and hippocampus. *Neuroscience* **146**, 9-16 (2007).
1107 https://doi.org/10.1016/j.neuroscience.2007.01.061
1108 63 Ardiles, A. O. *et al.* Pannexin 1 regulates bidirectional hippocampal synaptic plasticity in
1109 adult mice. *Front Cell Neurosci* **8**, 326 (2014). https://doi.org/10.3389/fncel.2014.00326
1110 64 Flores-Munoz, C. *et al.* The Long-Term Pannexin 1 Ablation Produces Structural and
1111 Functional Modifications in Hippocampal Neurons. *Cells* **11** (2022).
1112 https://doi.org/10.3390/cells11223646
1113 65 Flores-Munoz, C. *et al.* Acute Pannexin 1 Blockade Mitigates Early Synaptic Plasticity
1114 Defects in a Mouse Model of Alzheimer's Disease. *Front Cell Neurosci* **14**, 46 (2020).
1115 https://doi.org/10.3389/fncel.2020.00046
1116 66 Vroman, R. *et al.* Extracellular ATP hydrolysis inhibits synaptic transmission by increasing
1117 ph buffering in the synaptic cleft. *PLoS Biol* **12**, e1001864 (2014).
1118 https://doi.org/10.1371/journal.pbio.1001864
1119 67 Kranz, K. *et al.* Expression of Pannexin1 in the outer plexiform layer of the mouse retina
1120 and physiological impact of its knockout. *J Comp Neurol* **521**, 1119-1135 (2013).
1121 https://doi.org/10.1002/cne.23223
1122 68 Cenedese, V. *et al.* Pannexin 1 Is Critically Involved in Feedback from Horizontal Cells to
1123 Cones. *Front Mol Neurosci* **10**, 403 (2017). https://doi.org/10.3389/fnmol.2017.00403
1124 69 Gajardo, I. *et al.* Lack of Pannexin 1 Alters Synaptic GluN2 Subunit Composition and
1125 Spatial Reversal Learning in Mice. *Front Mol Neurosci* **11**, 114 (2018).
1126 https://doi.org/10.3389/fnmol.2018.00114
1127 70 Boyce, A. K., Kim, M. S., Wicki-Stordeur, L. E. & Swayne, L. A. ATP stimulates pannexin 1
1128 internalization to endosomal compartments. *Biochem J* **470**, 319-330 (2015).
1129 https://doi.org/10.1042/BJ20141551
1130 71 Boyce, A. K. J. & Swayne, L. A. P2X7 receptor cross-talk regulates ATP-induced pannexin
1131 1 internalization. *Biochem J* **474**, 2133-2144 (2017).
1132 https://doi.org/10.1042/BCJ20170257
1133 72 Bialecki, J. *et al.* Suppression of Presynaptic Glutamate Release by Postsynaptic
1134 Metabotropic NMDA Receptor Signalling to Pannexin-1. *J Neurosci* **40**, 729-742 (2020).
1135 https://doi.org/10.1523/JNEUROSCI.0257-19.2019
1136 73 Garcia-Rojas, F. *et al.* Pannexin-1 Modulates Inhibitory Transmission and Hippocampal
1137 Synaptic Plasticity. *Biomolecules* **13** (2023). https://doi.org/10.3390/biom13060887
1138 74 Siu, R. C. F., Kotova, A., Timonina, K., Zoidl, C. & Zoidl, G. R. Convergent NMDA receptor-
1139 Pannexin1 signaling pathways regulate the interaction of CaMKII with Connexin-36.
1140 *Commun Biol* **4**, 702 (2021). https://doi.org/10.1038/s42003-021-02230-x
1141 75 Cai, Q. & Tammineni, P. Mitochondrial Aspects of Synaptic Dysfunction in Alzheimer's
1142 Disease. *J Alzheimers Dis* **57**, 1087-1103 (2017). https://doi.org/10.3233/JAD-160726

1143 76 Henrich, M. T., Oertel, W. H., Surmeier, D. J. & Geibl, F. F. Mitochondrial dysfunction in
1144 Parkinson's disease - a key disease hallmark with therapeutic potential. *Mol*
1145 *Neurodegener* **18**, 83 (2023). https://doi.org/10.1186/s13024-023-00676-7
1146 77 Gao, X. Y., Yang, T., Gu, Y. & Sun, X. H. Mitochondrial Dysfunction in Parkinson's Disease:
1147 From Mechanistic Insights to Therapy. *Front Aging Neurosci* **14**, 885500 (2022).
1148 https://doi.org/10.3389/fnagi.2022.885500
1149 78 Zhao, J. *et al.* The Impact of Mitochondrial Dysfunction in Amyotrophic Lateral Sclerosis.
1150 *Cells* **11** (2022). https://doi.org/10.3390/cells11132049
1151 79 Liu, T. *et al.* Modulation of synaptic plasticity, motor unit physiology, and TDP-43
1152 pathology by CHCHD10. *Acta Neuropathol Commun* **10**, 95 (2022).
1153 https://doi.org/10.1186/s40478-022-01386-9
1154 80 Raefsky, S. M. & Mattson, M. P. Adaptive responses of neuronal mitochondria to
1155 bioenergetic challenges: Roles in neuroplasticity and disease resistance. *Free Radic Biol*
1156 *Med* **102**, 203-216 (2017). https://doi.org/10.1016/j.freeradbiomed.2016.11.045
1157 81 Sawant, N., Morton, H., Kshirsagar, S., Reddy, A. P. & Reddy, P. H. Mitochondrial
1158 Abnormalities and Synaptic Damage in Huntington's Disease: a Focus on Defective
1159 Mitophagy and Mitochondria-Targeted Therapeutics. *Mol Neurobiol* **58**, 6350-6377
1160 (2021). https://doi.org/10.1007/s12035-021-02556-x
1161 82 Dahl, G. The Pannexin1 membrane channel: distinct conformations and functions. *FEBS*
1162 *Lett* **592**, 3201-3209 (2018). https://doi.org/10.1002/1873-3468.13115
1163 83 Mim, C., Perkins, G. & Dahl, G. Structure versus function: Are new conformations of
1164 pannexin 1 yet to be resolved? *J Gen Physiol* **153** (2021).
1165 https://doi.org/10.1085/jgp.202012754
1166 84 Anderson, C. L. & Thompson, R. J. Intrapore lipids hydrophobically gate pannexin-1
1167 channels. *Sci Signal* **15**, eabn2081 (2022). https://doi.org/10.1126/scisignal.abn2081
1168 85 Hoeffer, C. A. & Klann, E. mTOR signaling: at the crossroads of plasticity, memory and
1169 disease. *Trends Neurosci* **33**, 67-75 (2010). https://doi.org/10.1016/j.tins.2009.11.003
1170 86 Bockaert, J. & Marin, P. mTOR in Brain Physiology and Pathologies. *Physiol Rev* **95**, 1157-
1171 1187 (2015). https://doi.org/10.1152/physrev.00038.2014
1172 87 Razani, E. *et al.* The PI3K/Akt signaling axis in Alzheimer's disease: a valuable target to
1173 stimulate or suppress? *Cell Stress Chaperones* **26**, 871-887 (2021).
1174 https://doi.org/10.1007/s12192-021-01231-3
1175 88 Heras-Sandoval, D., Perez-Rojas, J. M., Hernandez-Damian, J. & Pedraza-Chaverri, J. The
1176 role of PI3K/AKT/mTOR pathway in the modulation of autophagy and the clearance of
1177 protein aggregates in neurodegeneration. *Cell Signal* **26**, 2694-2701 (2014).
1178 https://doi.org/10.1016/j.cellsig.2014.08.019
1179 89 Adriaanse, B. A. *et al.* Tuberous sclerosis complex-1 (TSC1) contributes to selective
1180 neuronal vulnerability in Alzheimer's disease. *Neuropathol Appl Neurobiol* **49**, e12904
1181 (2023). https://doi.org/10.1111/nan.12904
1182 90 Liu, A. J. *et al.* Tuberous sclerosis complex is a novel, amyloid-independent tauopathy
1183 associated with elevated phosphorylated 3R/4R tau aggregation. *Acta Neuropathol*
1184 *Commun* **10**, 27 (2022). https://doi.org/10.1186/s40478-022-01330-x
1185 91 Safarian N., H.-T. S., Zoidl C., Zoidl G.R. Panx1b modulates the luminance response and
1186 direction of motion in the zebrafish. *BioRxiv* **BIORXIV-2021-453251v1-Zoidl** (2021).

1187 92 Safarian, N., Houshangi-Tabrizi, S., Zoidl, C., & Zoidl, G.R. . Panx1b Modulates the
1188 Luminance Response and Direction of Locomotion in the Zebrafish. *Int. J. Mol. Sci.*
1189 (2021). https://doi.org/https://doi.org/10.3390/ijms222111750
1190 93 MacPhail, R. C. *et al.* Locomotion in larval zebrafish: Influence of time of day, lighting and
1191 ethanol. *Neurotoxicology* **30**, 52-58 (2009). https://doi.org/10.1016/j.neuro.2008.09.011
1192 94 Safarian, N., Houshangi-Tabrizi, S., Zoidl, C. & Zoidl, G. R. Panx1b Modulates the
1193 Luminance Response and Direction of Locomotion in the Zebrafish. *Int J Mol Sci* **22**
1194 (2021). https://doi.org/10.3390/ijms222111750
1195 95 Baraban, S. C. Forebrain electrophysiological recording in larval zebrafish. *J Vis Exp*
1196 (2013). https://doi.org/10.3791/50104
1197 96 McCarthy, D. J., Chen, Y. & Smyth, G. K. Differential expression analysis of multifactor
1198 RNA-Seq experiments with respect to biological variation. *Nucleic Acids Res* **40**, 4288-
1199 4297 (2012). https://doi.org/10.1093/nar/gks042
1200 97 Robinson, M. D., McCarthy, D. J. & Smyth, G. K. edgeR: a Bioconductor package for
1201 differential expression analysis of digital gene expression data. *Bioinformatics* **26**, 139-
1202 140 (2010). https://doi.org/10.1093/bioinformatics/btp616
1203 98 Abad Tan, S., Zoidl, G. & Ghafar-Zadeh, E. A Multidisciplinary Approach Toward High
1204 Throughput Label-Free Cytotoxicity Monitoring of Superparamagnetic Iron Oxide
1205 Nanoparticles. *Bioengineering (Basel)* **6** (2019).
1206 https://doi.org/10.3390/bioengineering6020052
1207 99 Seal, R. L. *et al.* Genenames.org: the HGNC resources in 2023. *Nucleic Acids Res* **51**,
1208 D1003-D1009 (2023). https://doi.org/10.1093/nar/gkac888
1209 100 Mudunuri, U., Che, A., Yi, M. & Stephens, R. M. bioDBnet: the biological database
1210 network. *Bioinformatics* **25**, 555-556 (2009).
1211 https://doi.org/10.1093/bioinformatics/btn654
1212